Computational growth of neurons

What is the objective of computational growth?

One of the objectives of computational neuroscience is to generate artificial models of the brain.

In order to generate accurate models of the brain, at the level of detailed single cells, we need to populate brain regions with accurate cell morphologies in order to reproduce activity of neurons and their connectivity

However, not sufficient data are available of sufficiently good quality

The objective of computational generation of cells (neurons, glial, other cells) is to recreate the properties of biological cells

What is the objective of computational growth?

Fully grown neocortex

Blue Brain Project

Traditional algorithms

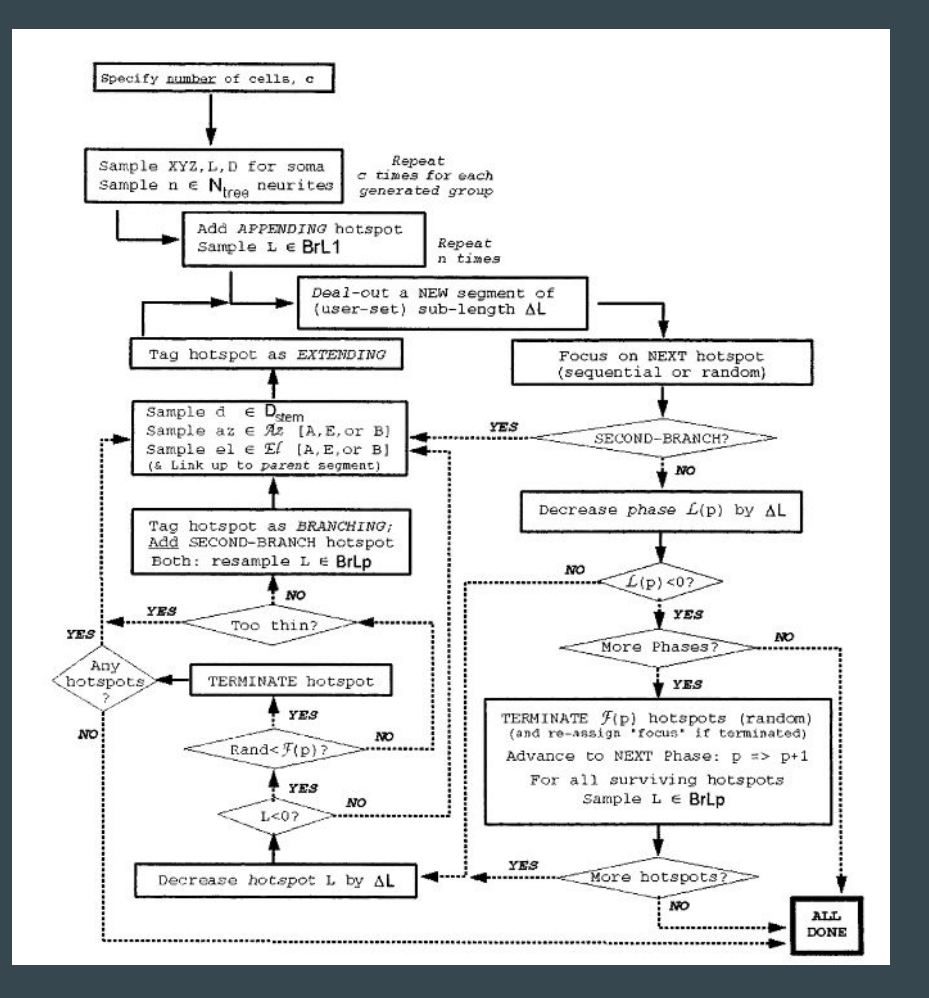
Traditionally, the computational generation of neurons started by a collection of simple rules with the aim to reproduce specific biological properties. For example, basic morphometrics:

- Number of branches
- Total length
- Maximum branch order
- Distribution of section lengths
- Distribution of angles

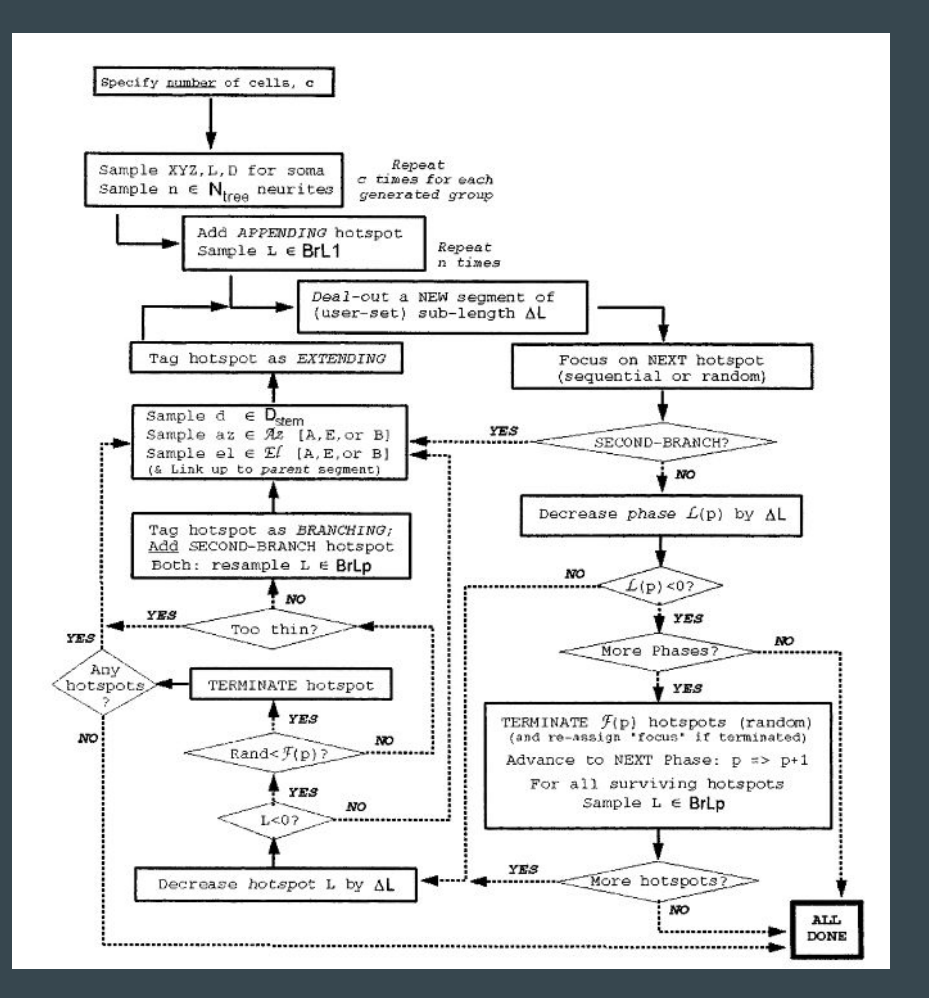
Were used as inputs to computational algorithms to generate neuronal morphologies

Computer generation and quantitative morphometric analysis of virtual neurons (Ascoli et al. 2001)

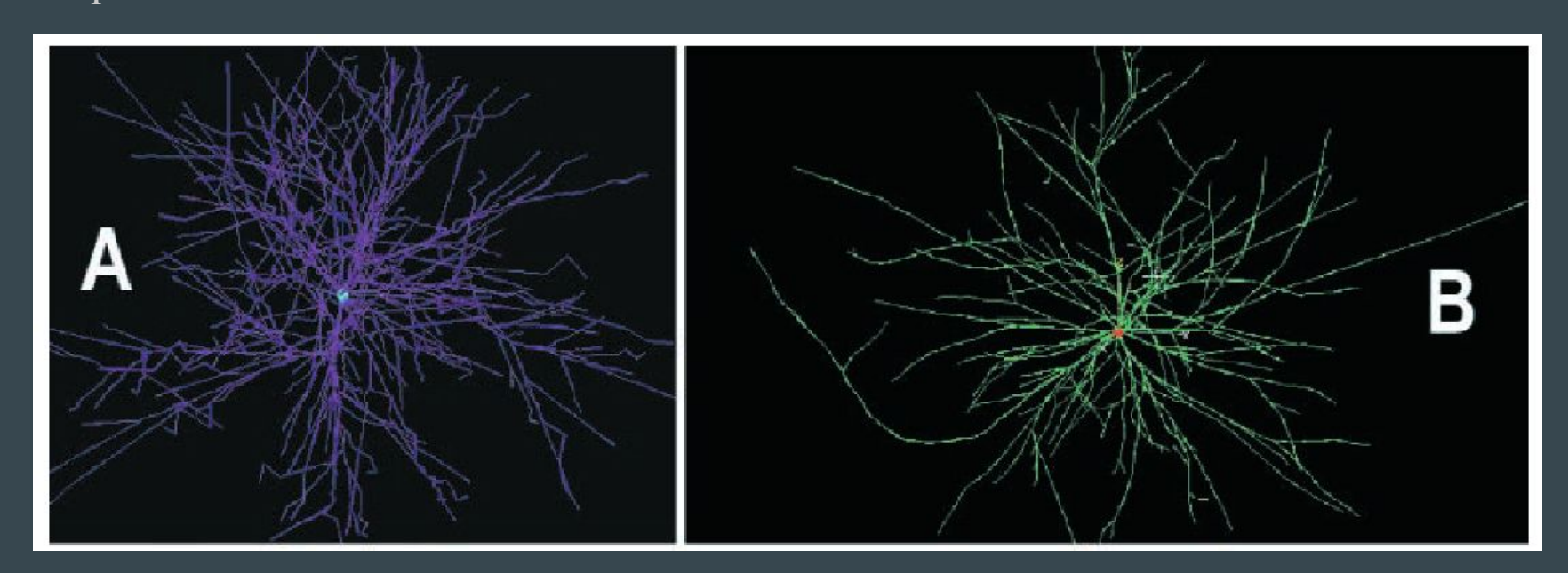
An important goal in computational neuroanatomy is the complete and accurate simulation of neuronal morphology. We are developing computational tools to model three-dimensional dendritic structures based on sets of stochastic rules.



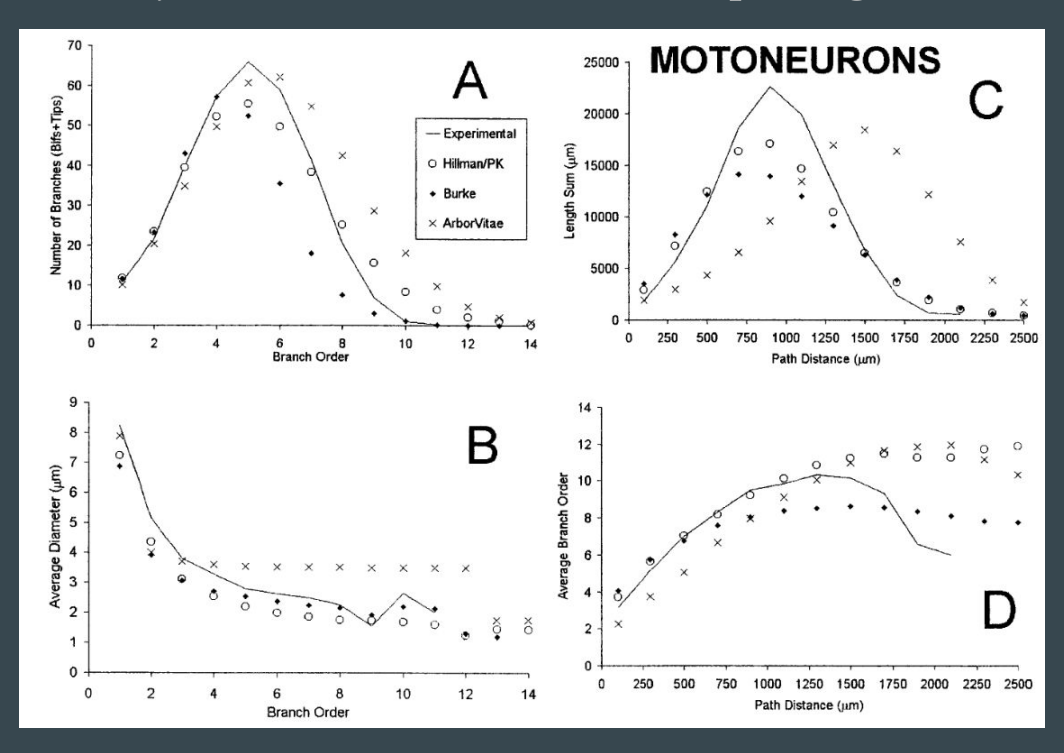
ArborVitae algorithm flow chart. The symbol p indicates the phase number. The total length per phase L(p) is calculated from the number of branches and their average length (BrLp*BrBp). The probability of termination F(p) is calculated from the numbers of terminations and bifurcations [BrTp/(BrTp+0.5*BrBp)].



Example of neurons that were generated based on the distribution of their morphometrics.

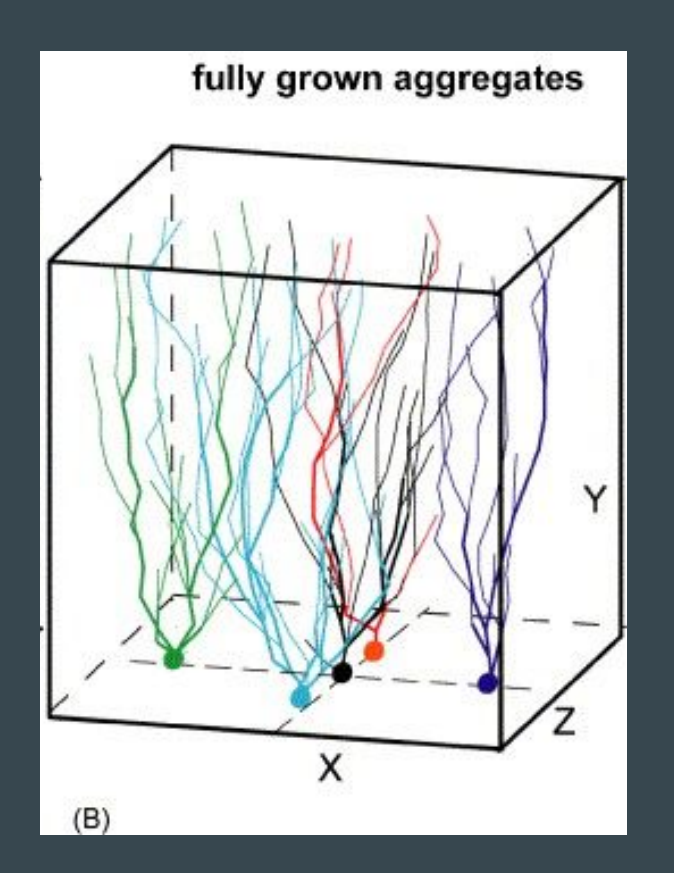


Statistical validation of synthesized motoneuron morphologies



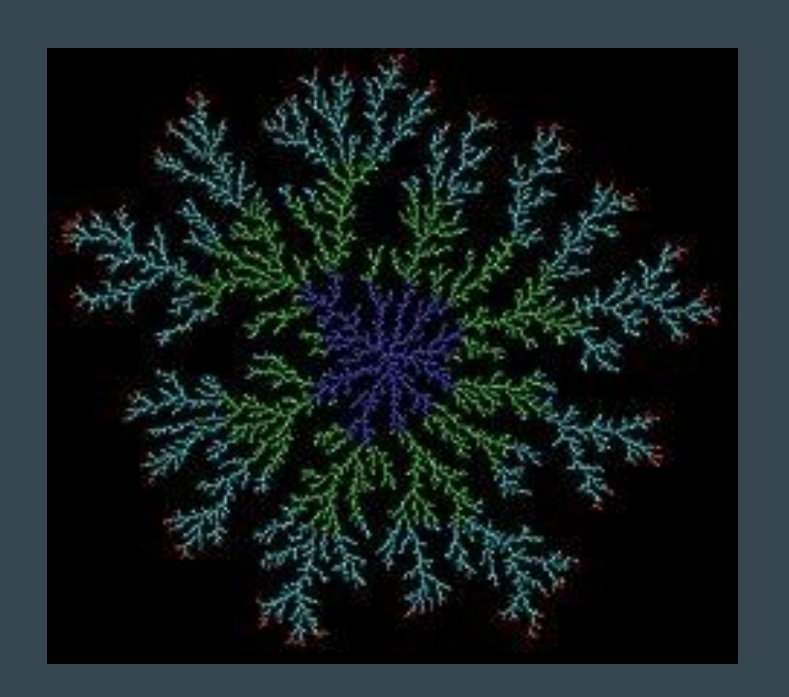
Spatial embedding of neuronal trees modeled by diffusive growth, Luczac 2006

The relative importance of the intrinsic and extrinsic factors determining the variety of geometric shapes exhibited by dendritic trees remains unclear. This question was addressed by developing a model of the growth of dendritic trees based on diffusion-limited aggregation process.



What is DLA?

Diffusion Limited Aggregation (DLA) is a "fractal" like pattern that emerges when particles move randomly and aggregate together. In DLA, particles are released into a space and move in straight lines until they collide with another particle or an aggregate. When a particle collides with an aggregate, it becomes a part of the aggregate and stops moving. Over time, as more particles are released, they continue to collide with the aggregate, causing it to grow in a fractal-like pattern.



Wikipedia

The shapes that can be generated based on this simple algorithms are not only artistically interesting, but can also approximate patterns that appear in biology:

Trees, Snowflakes, Neurons?

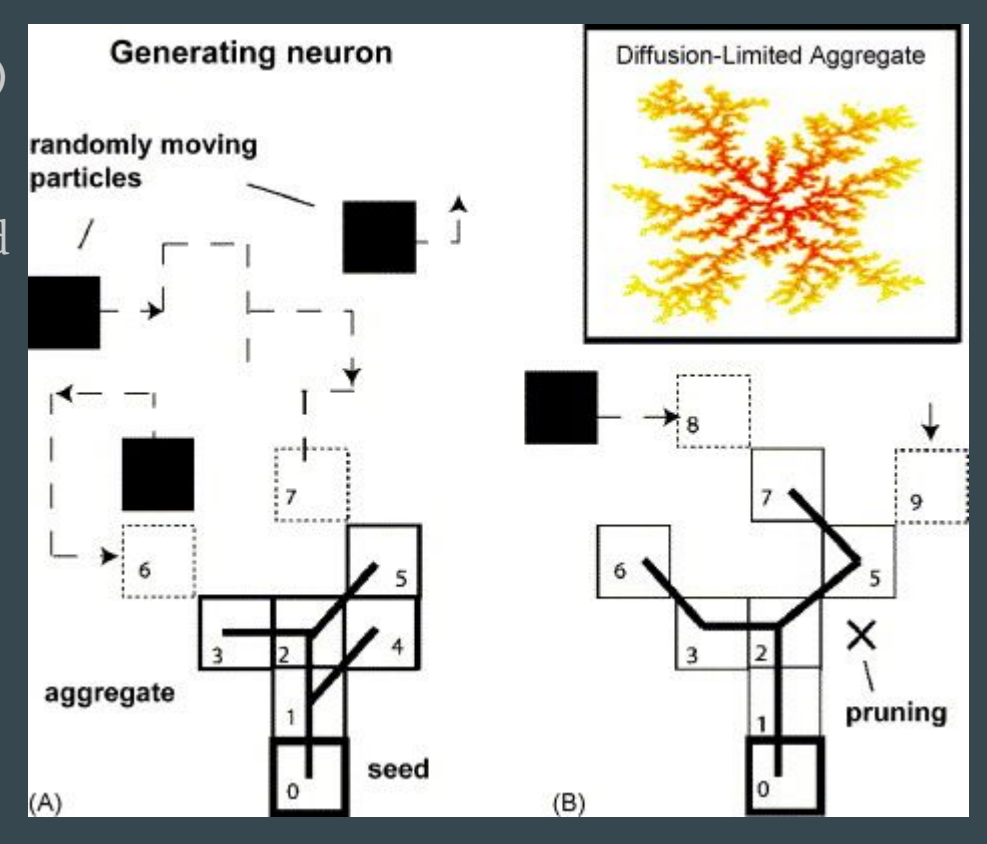




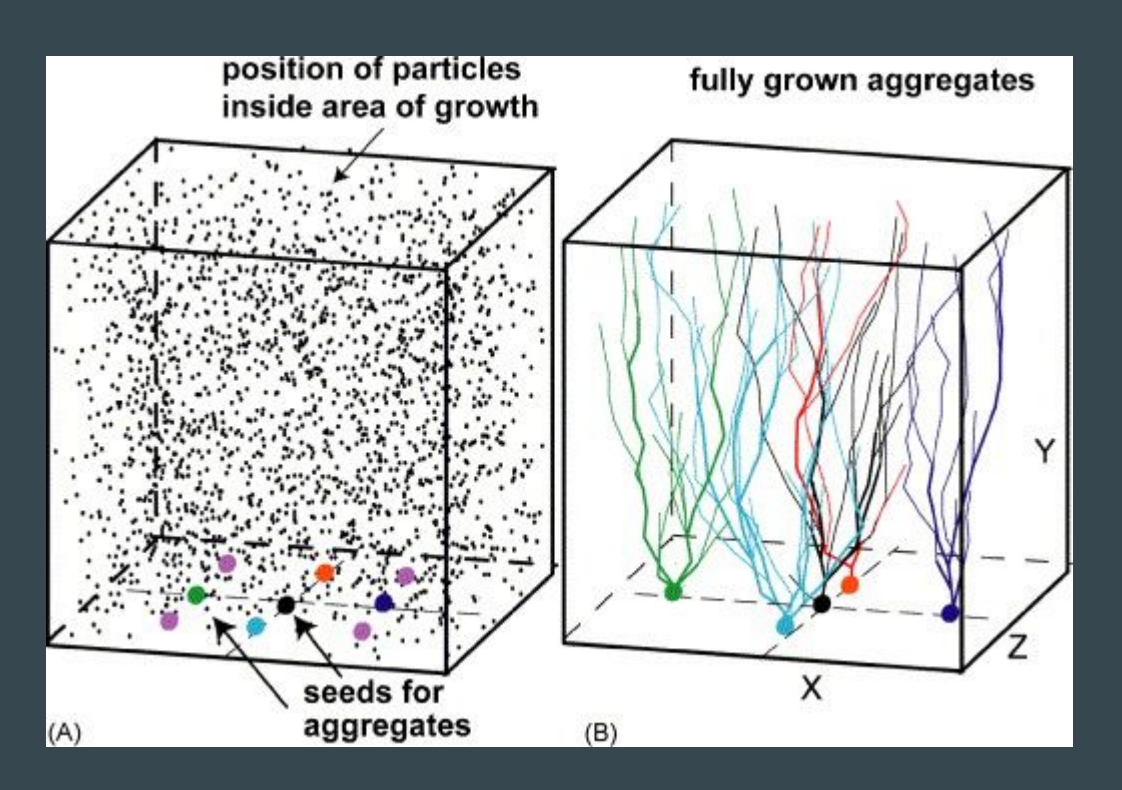
Wikipedia



Illustration of the DLA algorithm. (A) Randomly moving particles (black) stick irreversibly at their point of first contact with the aggregate (composed of particles 0–5). To each newly jointed particle a parent particle is assigned and both become connected by a line segment. (B) While the aggregate grows, the particles at the terminals are randomly deleted from the aggregate (pruning) during a specified time window.

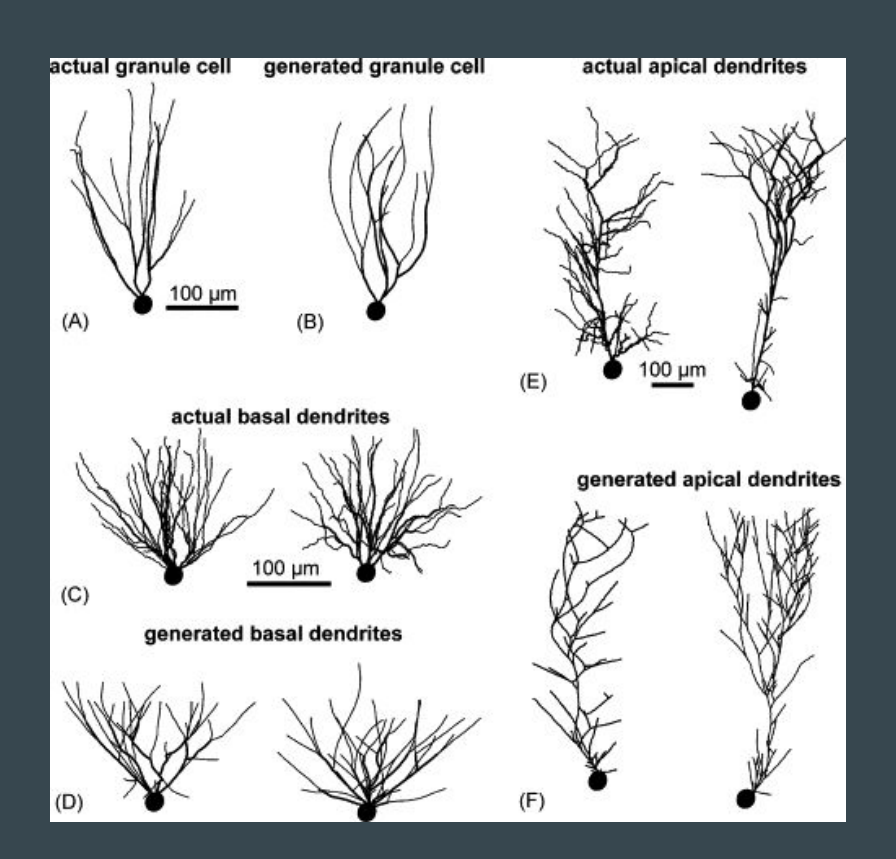


Generating neurons in ensemble. (A) Illustration of the initial condition for generating nine aggregates. (B) Generated granule cells (cells in corners are not shown for visualization clarity). Rectangular box represents a space limitation imposed on the growth of aggregates.



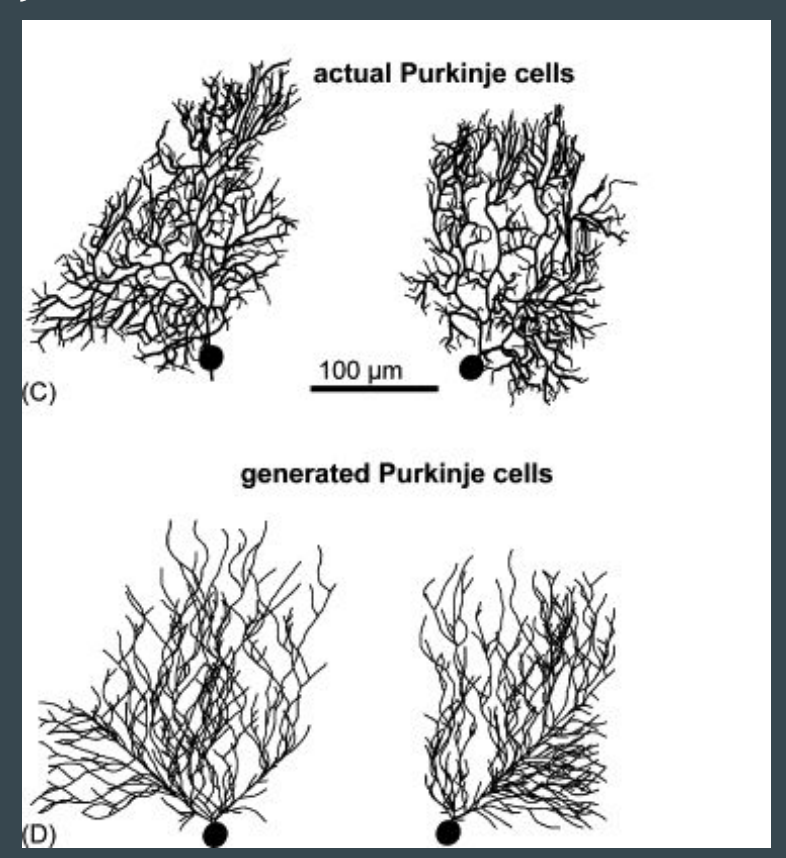
Examples of real and generated neurons. (A and B) Examples of real and generated granule cells. (C and D) Examples of real and generated basal dendrites. (E and F) Examples of real and generated apical dendrites of pyramidal cells. The cell bodies are depicted by spheres.

The outgrowth properties are nicely captured, but the local details of more complex cells are hard to capture.

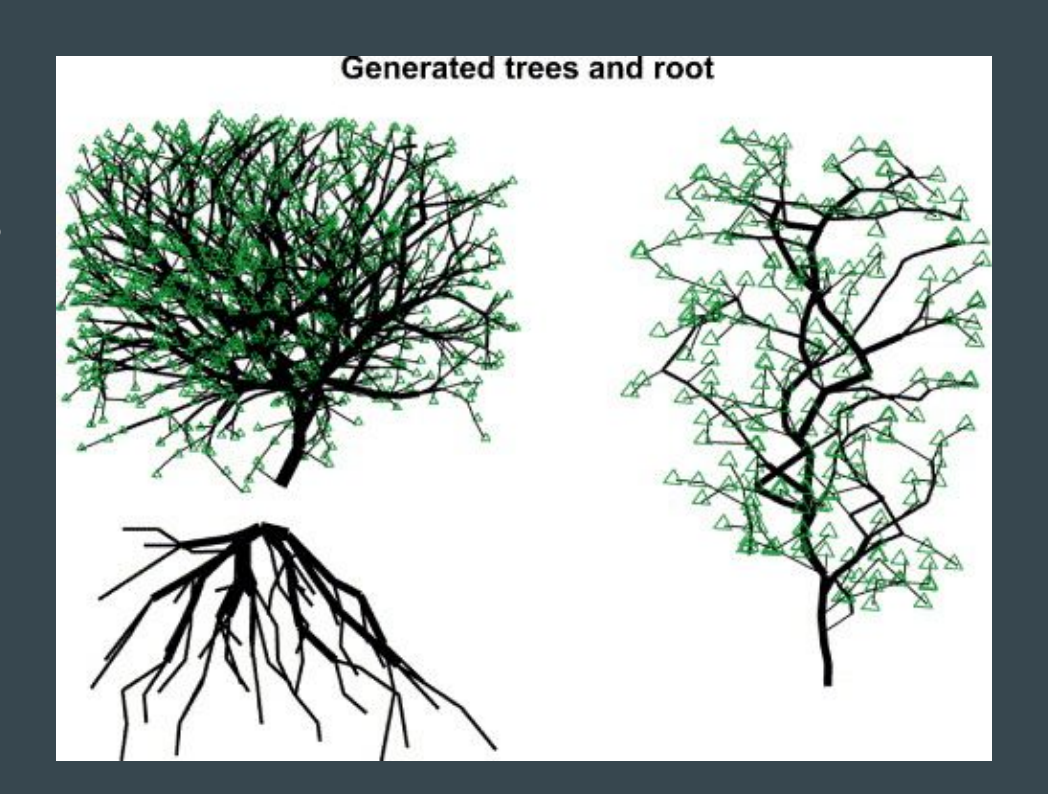


Examples of real and generated neurons. (A and B) Examples of real and generated axonal trees of interneurons. (C and D) Examples of real and generated Purkinje cells. The cell bodies are depicted by spheres.

Symmetrics properties of the trees are better captured by this algorithm



Demonstration of the general applicability of the algorithm to model diverse types of tree structures (from left: pear tree, root and hornbeam; terminal branches are depicted as triangles to resemble leaves).



TREES algorithm

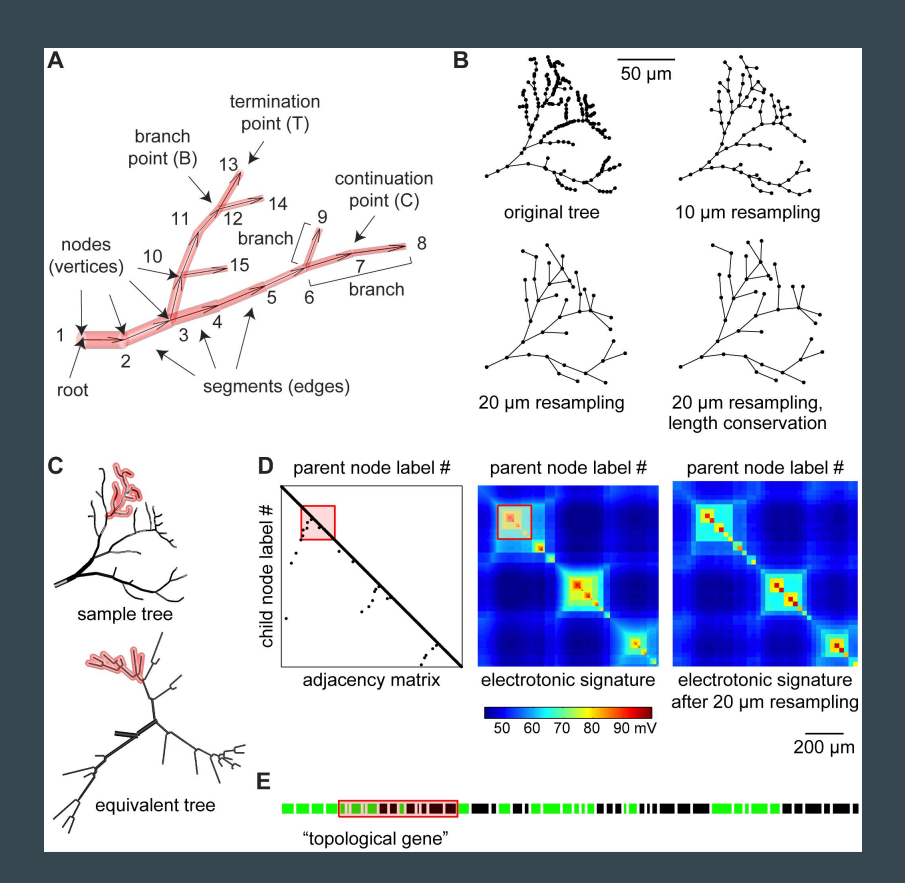
One Rule to Grow Them All: A General Theory of Neuronal Branching and Its Practical Application

Cuntz et al. 2010

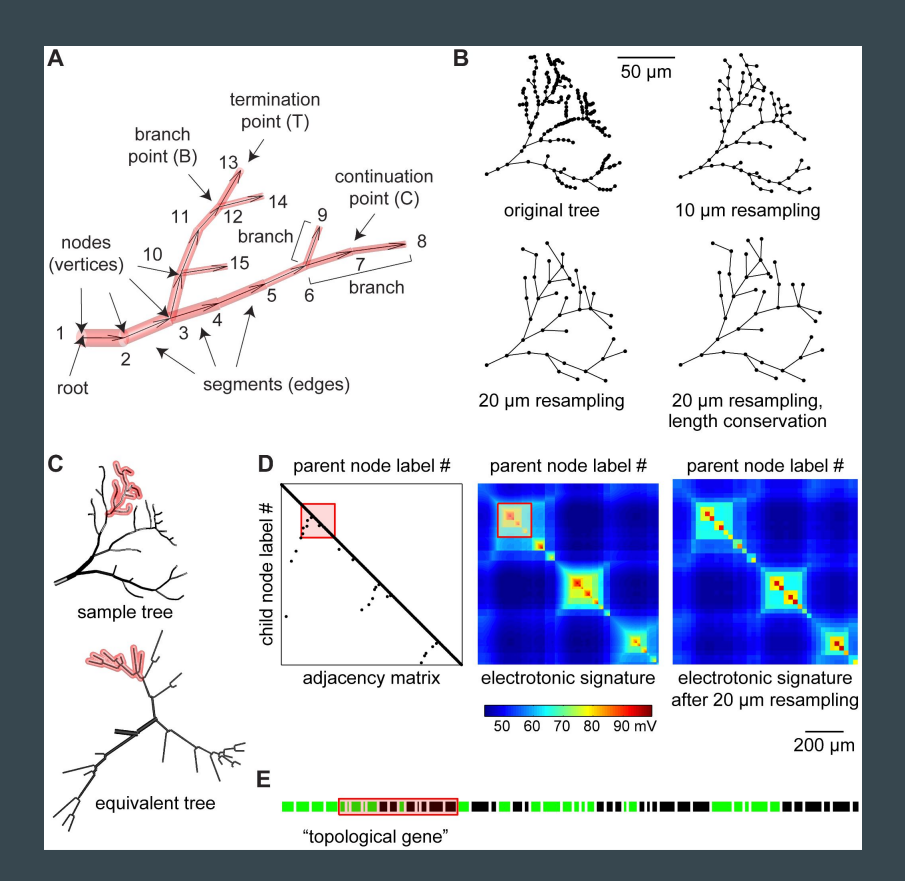
One Rule to Grow Them All: A General Theory of Neuronal Branching and Its Practical Application

Understanding the principles governing axonal and dendritic branching is essential for unravelling the functionality of single neurons and the way in which they connect. Nevertheless, no formalism has yet been described which can capture the general features of neuronal branching. Here we propose such a formalism, which is derived from the expression of dendritic arborizations as locally optimized graphs. Inspired by Ramo 'n y Cajal's laws of conservation of cytoplasm and conduction time in neural circuitry, we show that this graphical representation can be used to optimize these variables. This approach allows us to generate synthetic branching geometries which replicate morphological features of any tested neuron. The essential structure of a neuronal tree is thereby captured by the density profile of its spanning field and by a single parameter, a balancing factor weighing the costs for material and conduction time. This balancing factor determines a neuron's electrotonic compartmentalization. Additions to this rule, when required in the construction process, can be directly attributed to developmental processes or a neuron's computational role within its neural circuit. The simulations presented here are implemented in an open-source software package, the "TREES toolbox," which provides a general set of tools for analyzing, manipulating, and generating dendritic structure, including a tool to create synthetic members of any particular cell group and an approach for a model-based supervised automatic morphological reconstruction from fluorescent image stacks. These approaches provide new insights into the constraints governing dendritic architectures. They also provide a novel framework for modelling and analyzing neuronal branching structures and for constructing realistic synthetic neural networks.

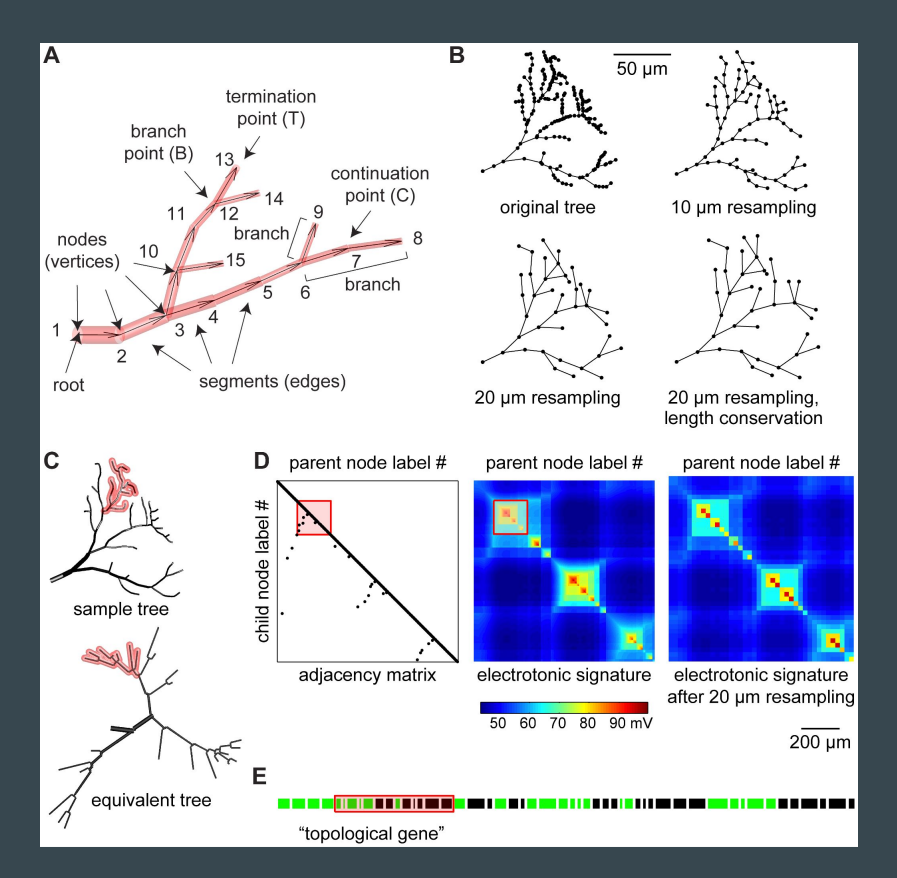
The connectivity and electrotonic properties of a neuronal tree. (A) The tree consists of cylinders or frusta (red) connecting each two nodes along the directed edges (away from the root node, arrows). Branch points and termination points represent the topology (topological points). A branch is a set of continuation points between two topological points. The labelling of the nodes is unique following three principles: hierarchical sorting, continuous labelling preserving sub-tree consistency and topological sorting (see text). (B) Rearrangement of node locations on a sample tree.

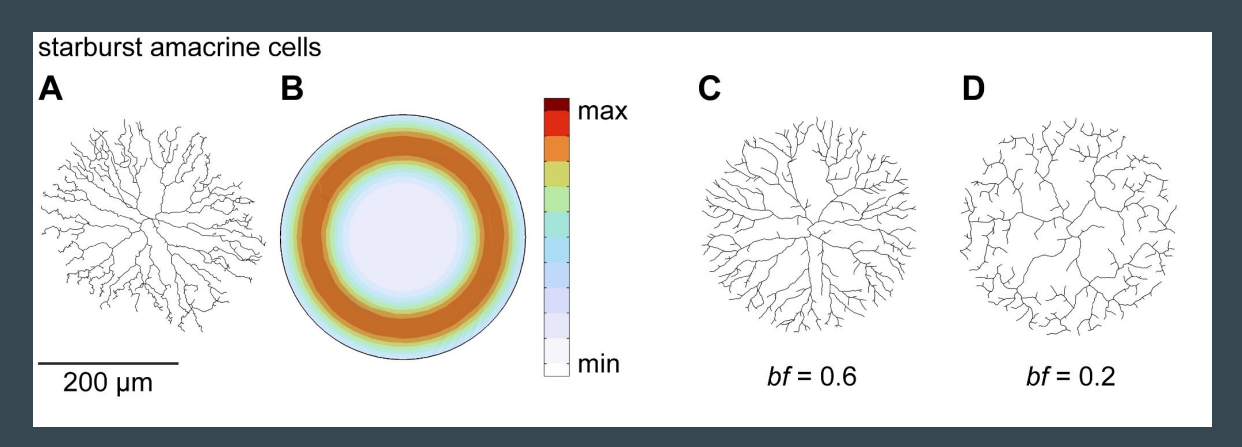


(C) Applying topological sorting, a unique electrotonic equivalent tree constructed by mapping node hierarchy on the branch angle (equivalent tree). (D) The adjacency matrix depicts the connectivity between the nodes of a tree. The corresponding electrotonic signature (current transfer from a node to another, i.e. the potential difference measured in one node as a result of a current injection into another) describes the dendritic compartmentalization (see text). The electrotonic signature corresponding to the um resampled tree preserves the compartmentalization of the original tree.

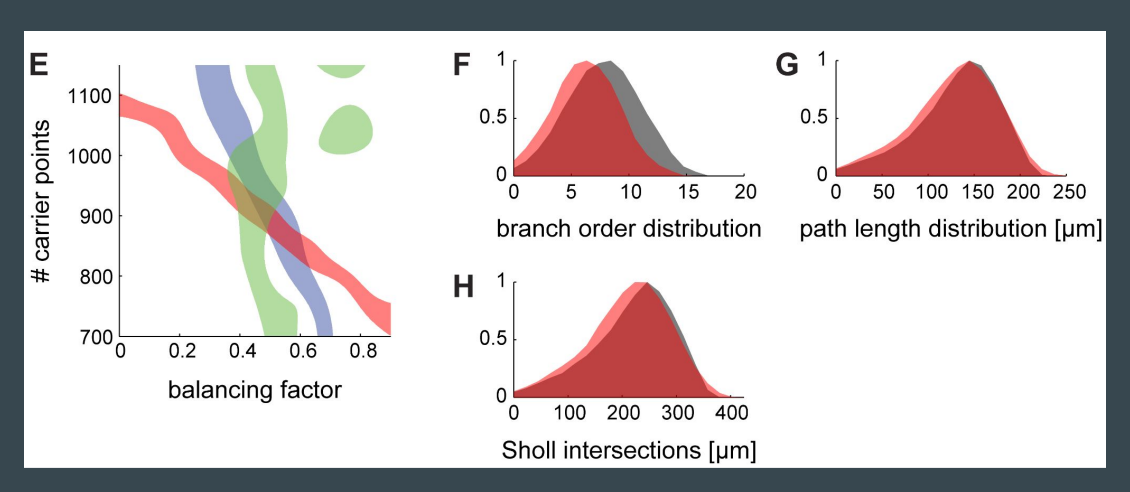


(E) A one-dimensional string fully describes the topology once the nodes of a tree are sorted topologically. Green pieces represent branches ending with a branch point while black pieces end with a termination point. Branch lengths correspond to real metric length and their order follows the node label sorting. Because all representations observe the same continuous labelling, they preserve the sub-tree structure (a red transparent patch highlights one such sub-tree throughout all representations in (C–E)).





Generating dendritic structures by constructing geometric spanning fields: I. the retinal starburst amacrine cell. (A) Reconstruction of a starburst amacrine cell in the inner plexiform layer of the rabbit retina (data from [24]). (B) Synthetic starburst amacrine cell morphologies can be best obtained by distributing random carrier points along a density ring limited by a circular hull. (C) An example tree grown on random carrier points distributed according to B following the algorithm described in Figure 2. Spatial jitter was added to reproduce the wriggliness of the original structure. (D) A tree grown on exactly the same points as (C) with a lower balancing factor.

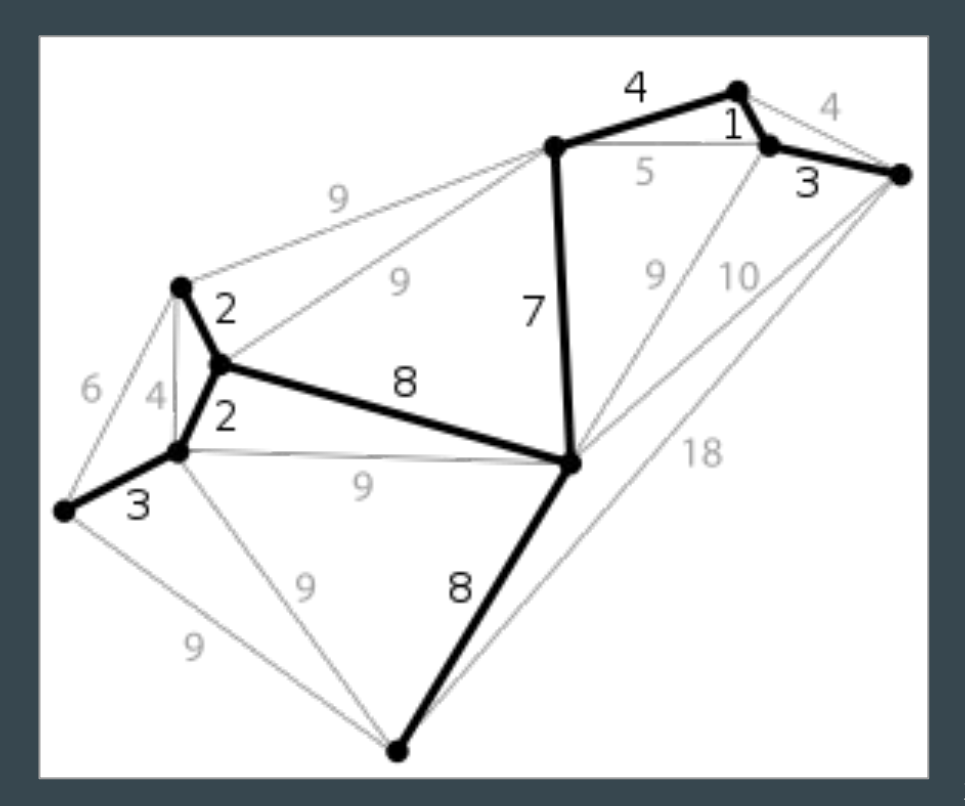


(E) The number of randomly distributed carrier points and the balancing factor bf determine the synthetically generated morphology. Here, the areas are plotted in which the synthetic trees match the original according to certain criteria (blue: total cable length ± 200 µm; red: total number of branch points ± 5 ; green: mean path length to the root ± 3 µm). The area of overlap corresponds to a reasonable parameter set for the synthetic trees. (F–H) Branch order distribution, path length distribution and Sholl intersections are compared for the original tree (red) and for one sample synthetic tree (grey).

Minimum spanning tree

Minimum spanning tree

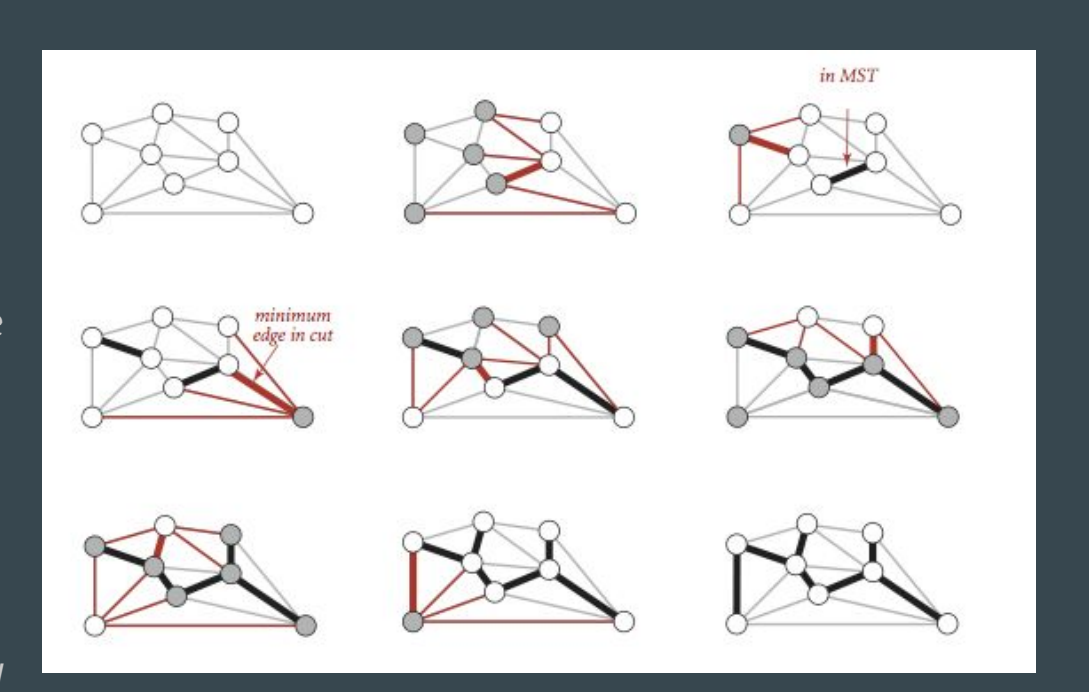
A minimum spanning tree (MST) is a subset of the edges of a connected, edge-weighted undirected graph that connects all the vertices together, without any cycles and with the minimum possible total path length.



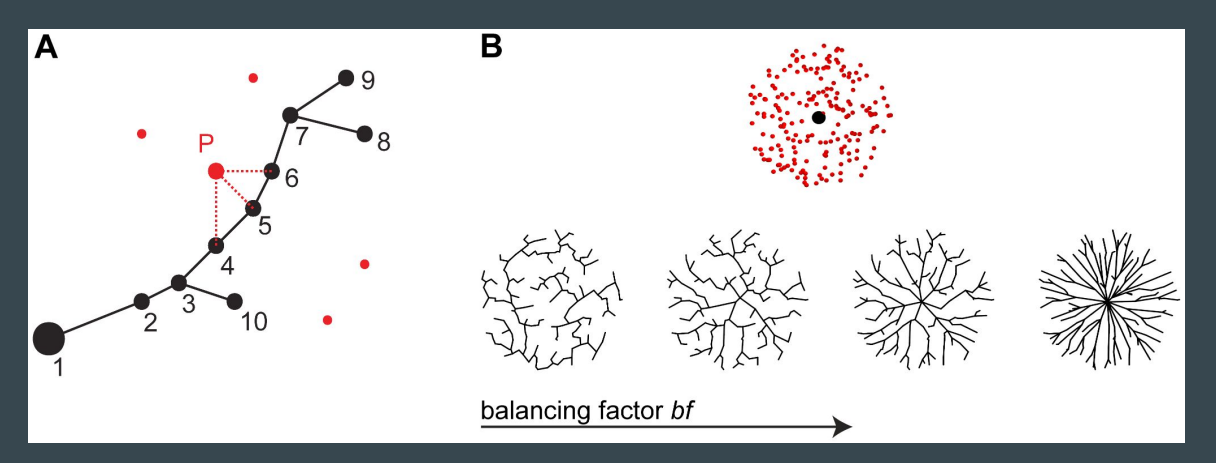
Minimum spanning tree

Example algorithm to generate MST from a graph

MST edge is the smallest for each set of edge cuts that disconnects the graph.

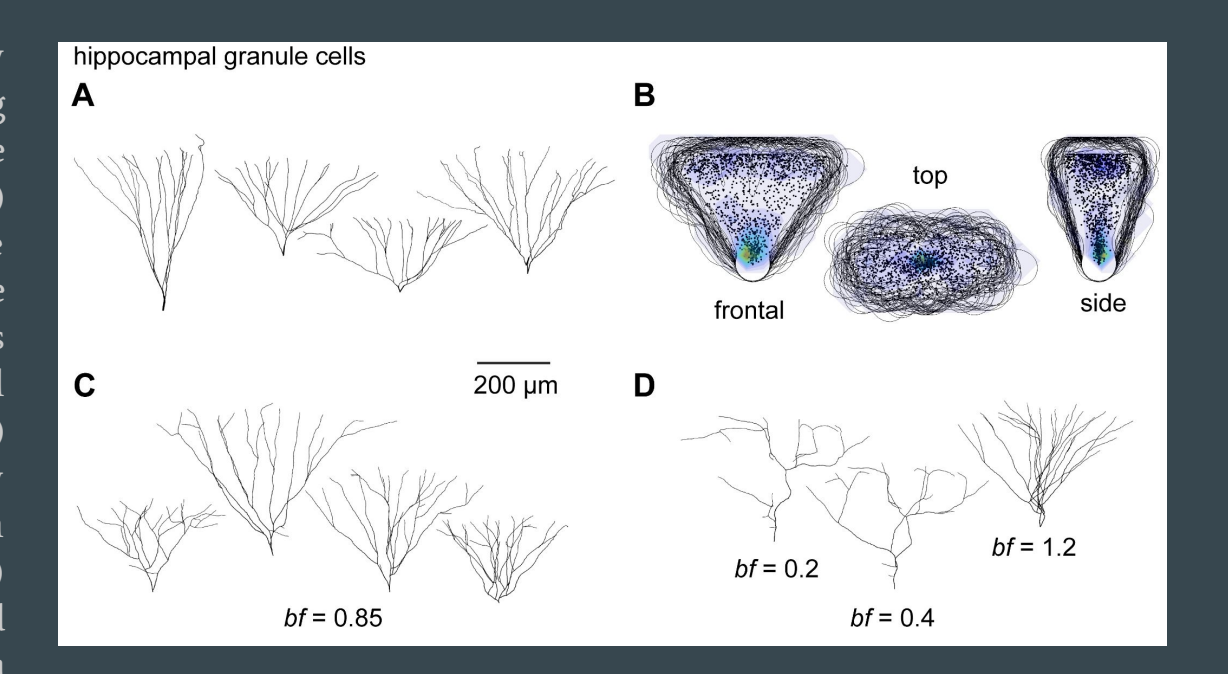


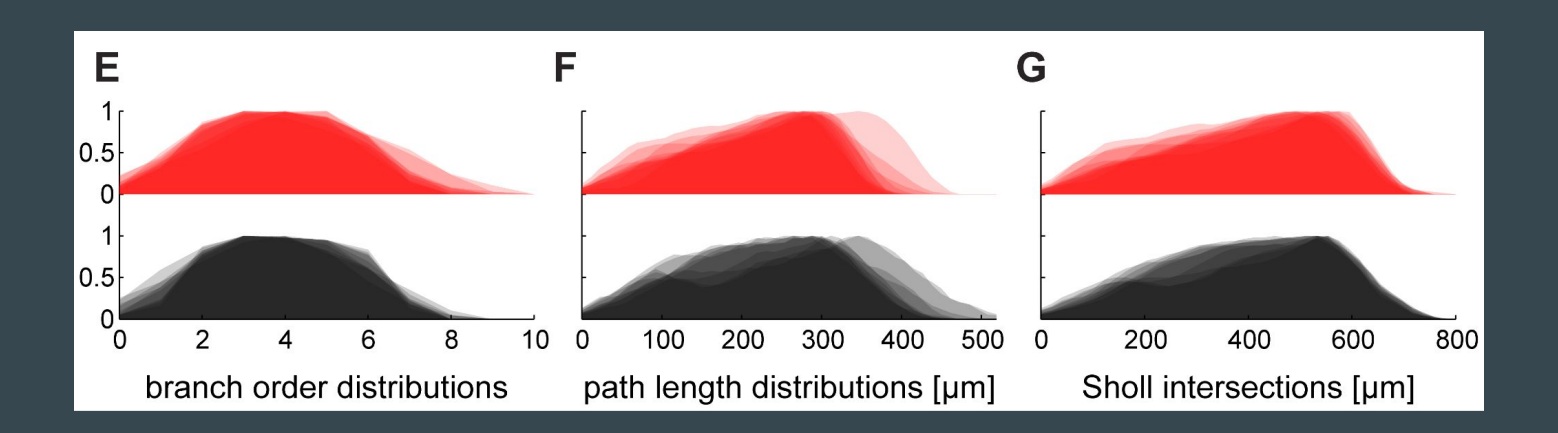
https://algs4.cs.princeton.edu/43mst/



Generating neuronal branching structures using optimized graphs. (A) The growth described by an extended minimum spanning tree algorithm (see text). Unconnected carrier points (red) are connected one by one to the nodes of a tree (black). Red dashed lines indicate three sample Euclidean distances to the nodes of the tree for sample point P. (B) Example trees grown on homogeneously distributed random carrier points in a circular hull starting from a root located at its centre (see top). Plotted as a function of the balancing factor bf, the trees range from perfect minimum spanning trees (left) to almost direct connections from the root to any point (right).

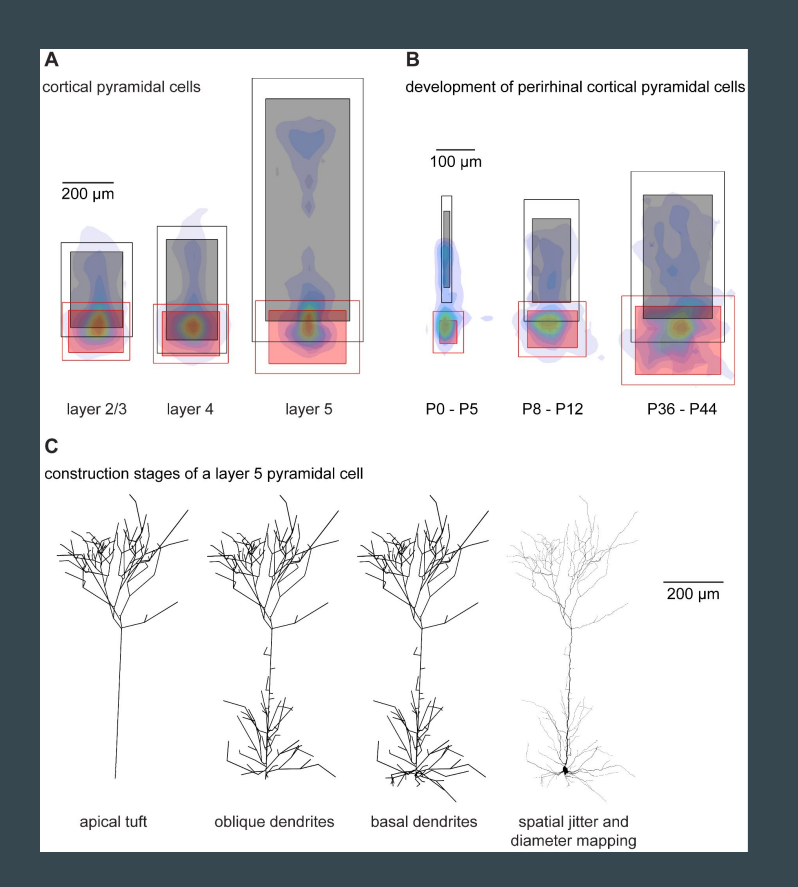
Generating dendritic structures by constructing geometric spanning fields: II. the hippocampal dentate granule cell. (A) gyrus Reconstructions of four sample hippocampal granule cells. (B) The 50 µm iso-distance volume hulls (black lines) around the set of all topological points (black dots) overlap in all dimensions. Overlay colours represent local density with same colormap as in Figure 3. (C) Examples of synthetically generated granule cells (based on the data in AB) with bf=0.85. (D)



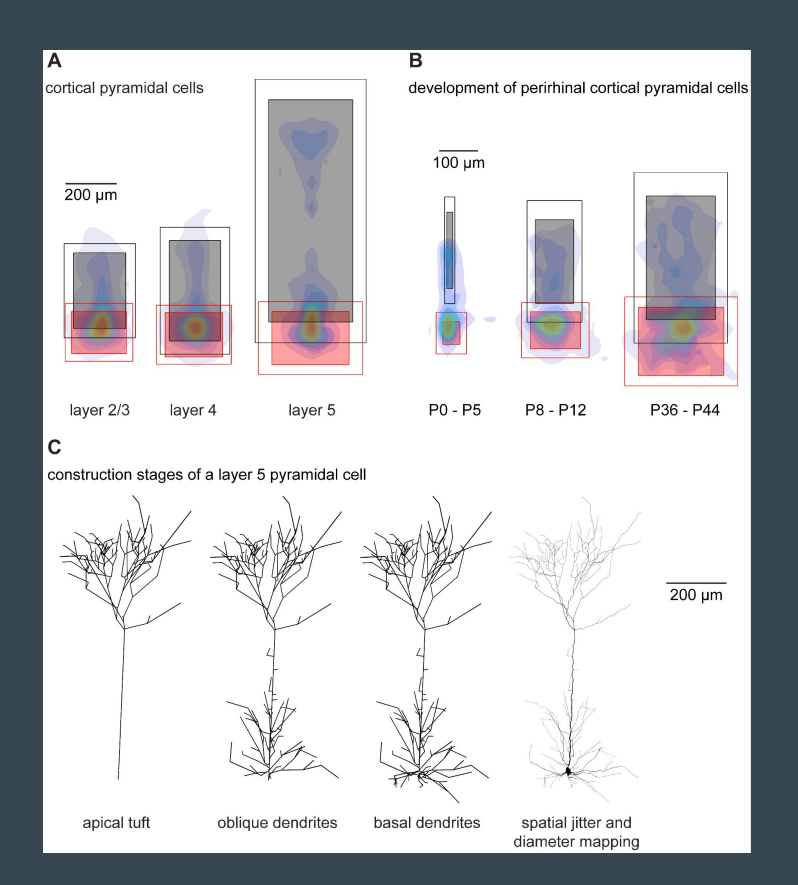


(E–G) Overlaid branch order distributions, path length distributions and Sholl intersections for original trees (red) and for synthetic trees with suitable parameter bf=0.85 (black).

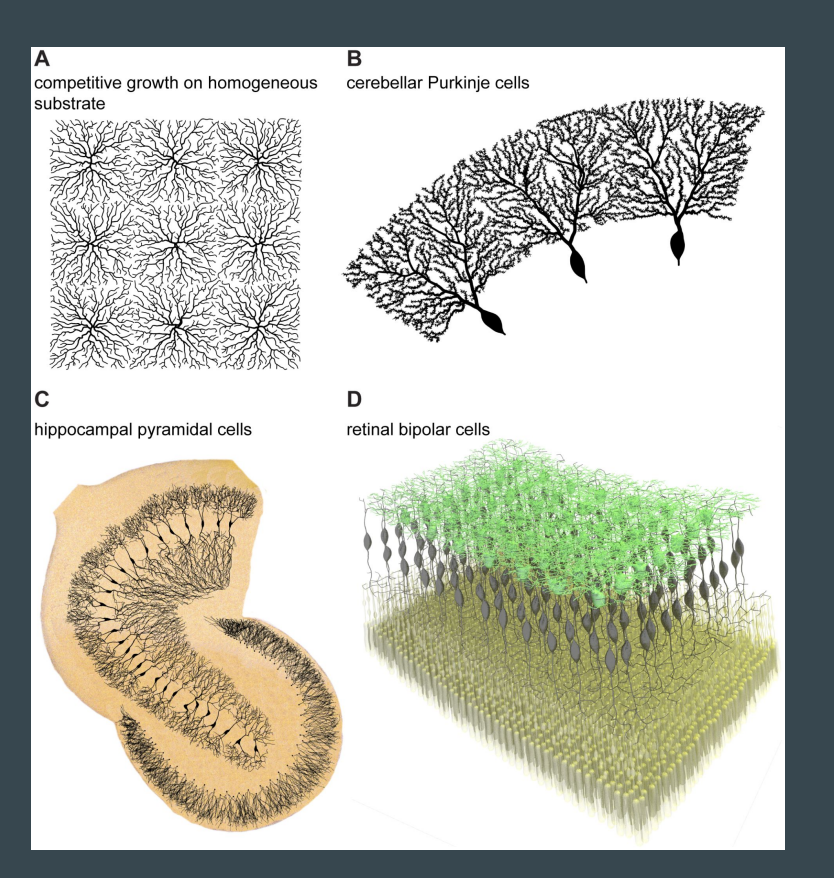
A general strategy for generating synthetic morphologies: Cortical pyramidal cells. (A) After rotating rat somatosensory cortex layer 2/3, 4 and 5 pyramidal cells to overlap, the limits of their individual regions were extracted: black shaded boxes show the mean limits in XY for the apical region; the black empty boxes delineate one standard deviation away from the mean. Corresponding red boxes duplicate this procedure for the basal dendrites.



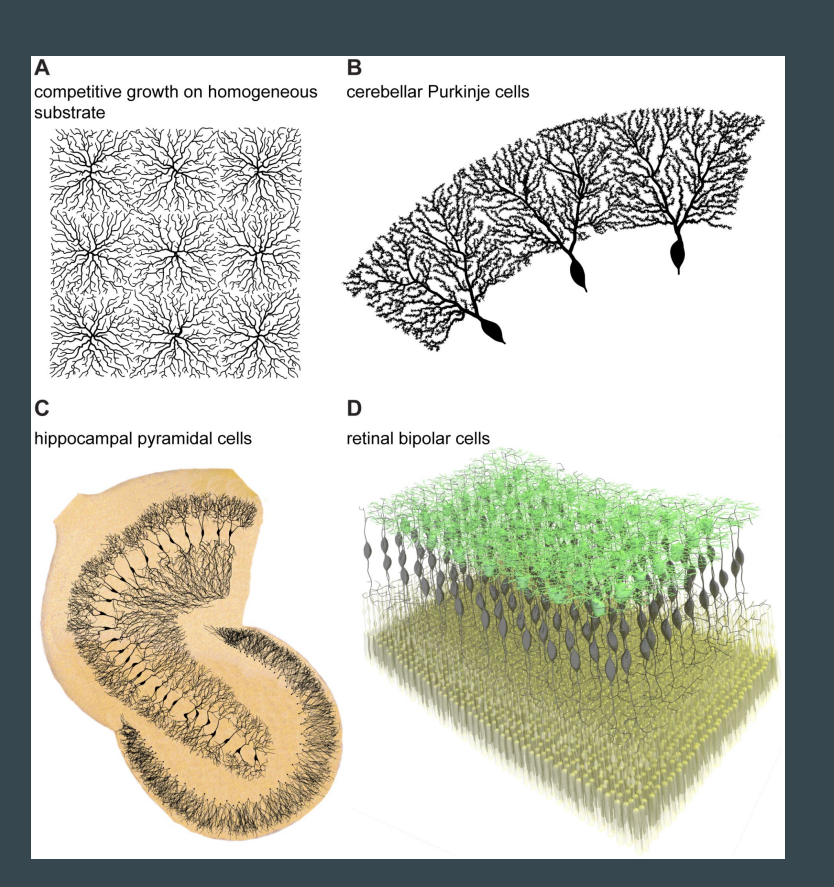
Cells are then scaled region-by-region to the mean limits of each region. Overlay colours describe local density (colormap see Figure 2D) of lumped topological points of scaled trees. (B) Same procedure for three groups of cortical pyramidal cells during development. (C) Construction stages of a sample layer 5 pyramidal cell according to spanning fields described in A. First the apical tuft is constructed, then oblique dendrites and finally the basal dendrite. Spatial jitter and diameter values are added subsequently.



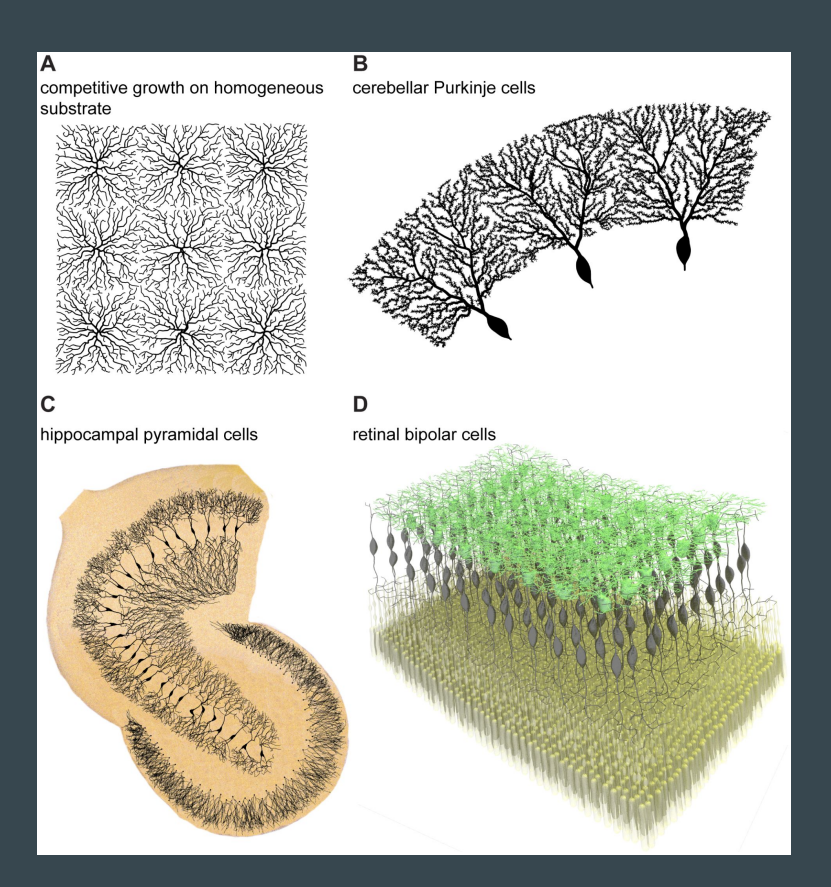
The interactions between neuronal branching and the network context. (A) Nine synthetic neuronal trees grown competitively on a sample square substrate of homogeneously distributed random carrier points: the competitive greedy growth results automatically in tiling of the available space. (B) Three out of 16 neuronal trees grown competitively on random carrier points distributed on a ring: this simulates well the sharp borders of Purkinje cells in the cerebellum. Whether Purkinje cell dendrites actually tile in sagittal planes of the cerebellum remains to be determined.



(C) Hippocampal granule cells from Figure 4 were scaled and positioned along the contours of a human dentate gyrus obtained from a sketch by Camillo Golgi [31]. Growing synthetic CA3 hippocampal pyramidal cells competitively with the limits from the template resulted in realistic hippocampal pyramidal cells affected by mutual avoidance. Synthetic dendrites were overlaid on the background of the original sketch.

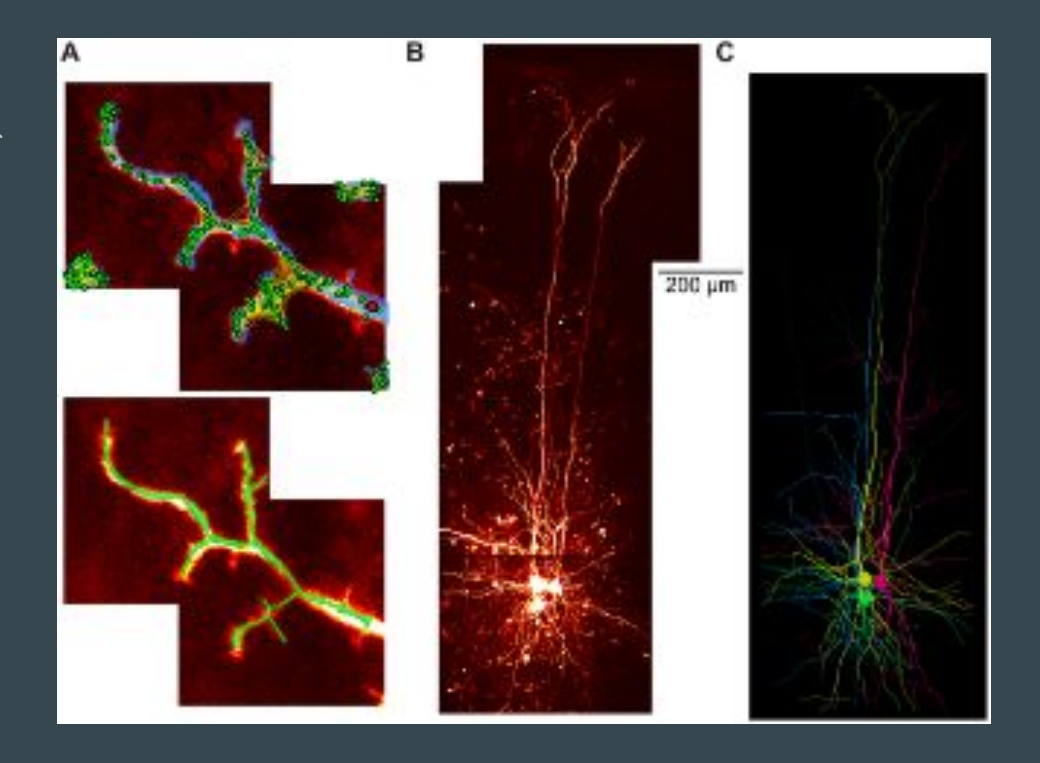


(D) Bipolar cells (black) in the retina were grown competitively to connect an array of photoreceptors (yellow) to an array of starburst amacrine cells (green, obtained using the algorithm in Figure 3). In such a case the full morphology of bipolar cells is determined by the context of the circuitry, after prescribing soma locations of the bipolar cells. For all panels of Figure 8 precise scale bars would depend on the details of the preparations and were therefore omitted.



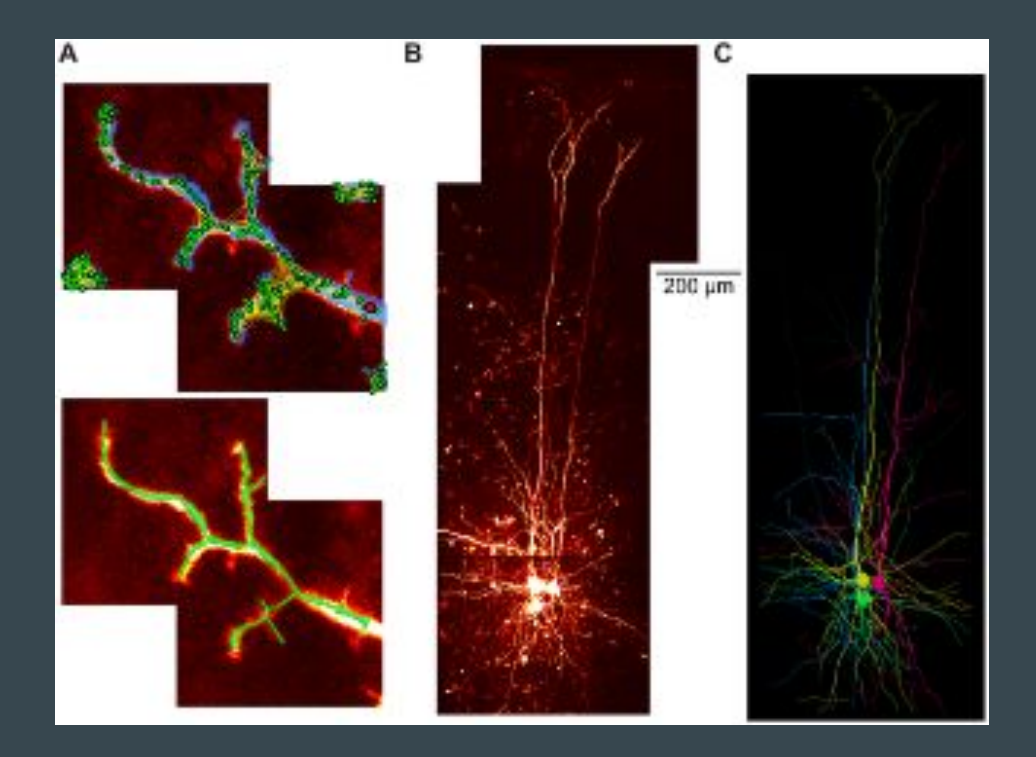
One Rule to Grow Them All

Automated reconstruction of multiple cells using the greedy algorithm. (A) Example of an additional application of the algorithm: automated model-based tree reconstruction from image stacks. Maximum intensity projection of tiled image stacks containing a sample sub-tree of a fluorescently labelled neuronal tree. The resulting binary matrix is then reduced to single points in space (green dots) via a skeletonization procedure. The points are used as carrier points for the growth algorithm to obtain the corresponding tree using the distance graph as an additional cost factor.



One Rule to Grow Them All

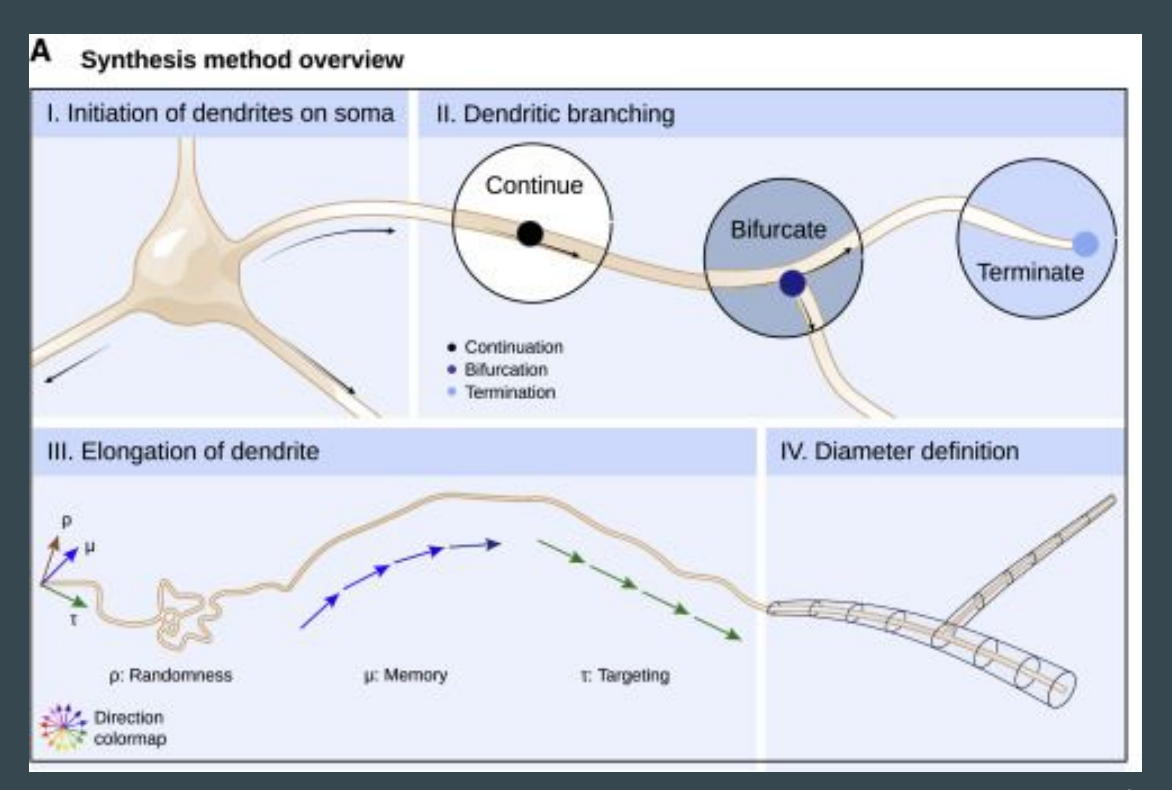
(B) Maximum intensity projections of tiled 2-photon fluorescent image stacks from primary visual cortex of a mouse expressing GFP in parvalbumin interneurons. Three layer 5 pyramidal neurons are also imaged; all cells were filled with a fluorescent dye Alexa 594 via whole cell patch-clamp recording. Data courtesy of Kate Buchanan and Jesper Sjöström. (C) Corresponding reconstructions (with the interneuron in green) grown in a competitive manner on the image stacks after manual post-processing.



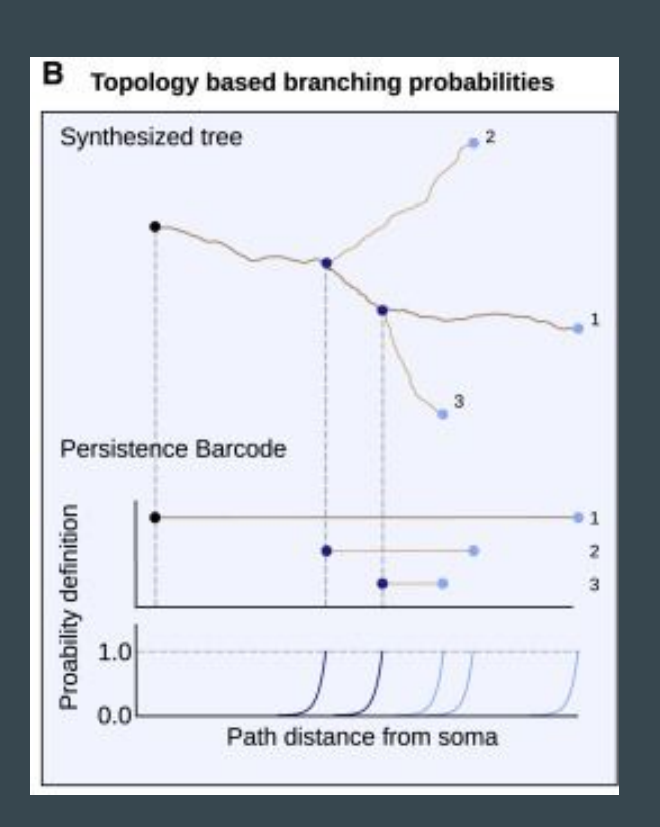
Kanari et al. 2022

Neuronal morphologies provide the foundation for the electrical behavior of neurons, the connectomes they form, and the dynamical properties of the brain. Comprehensive neuron models are essential for defining cell types, discerning their functional roles, and investigating brain-disease-related dendritic alterations. However, a lack of understanding of the principles underlying neuron morphologies has hindered attempts to computationally synthesize morphologies for decades. We introduce a synthesis algorithm based on a topological descriptor of neurons, which enables the rapid digital reconstruction of entire brain regions from few reference cells. This topology-guided synthesis generates dendrites that are statistically similar to biological reconstructions in terms of morpho-electrical and connectivity properties and offers a significant opportunity to investigate the links between neuronal morphology and brain function across different spatiotemporal scales. Synthesized cortical networks based on structurally altered dendrites associated with diverse brain pathologies revealed principles linking branching properties to the structure of large-scale networks.

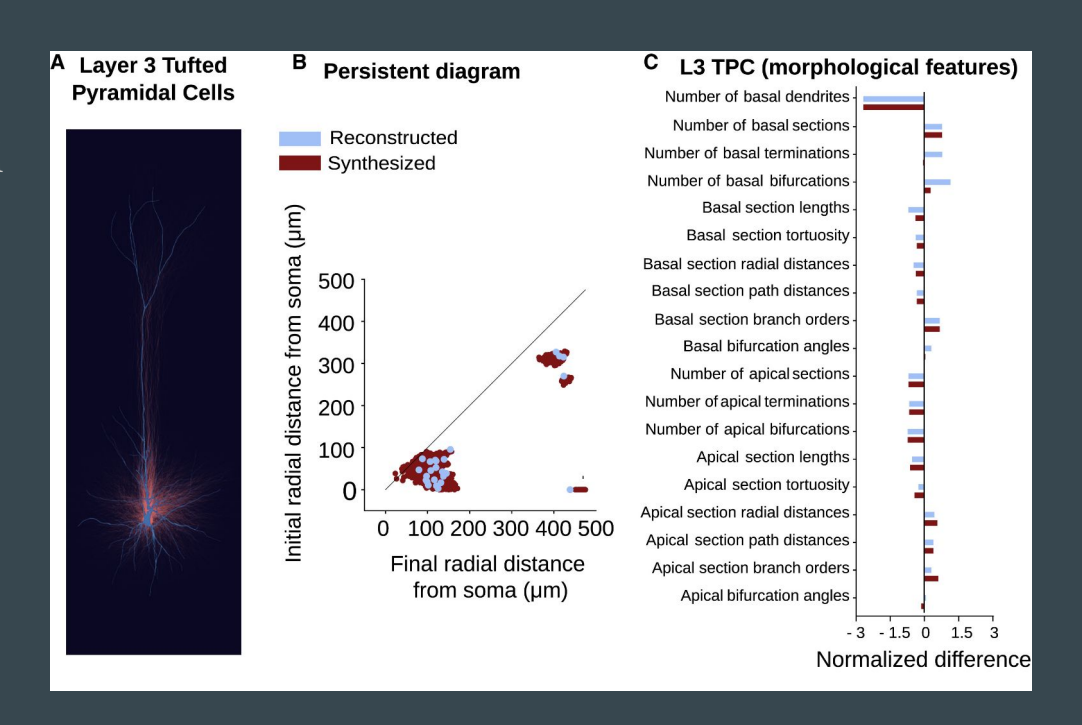
(A) Overview of dendritic synthesis based on four stages of growth. (I) Soma generation and initiation of the dendrites on the soma surface. (II) Stochastic definition of bifurcation, termination, and elongation (III) based on topological descriptor. (IV) Diameter definition, as a final step, is based on the biological distributions and is subsequent to the branching steps.



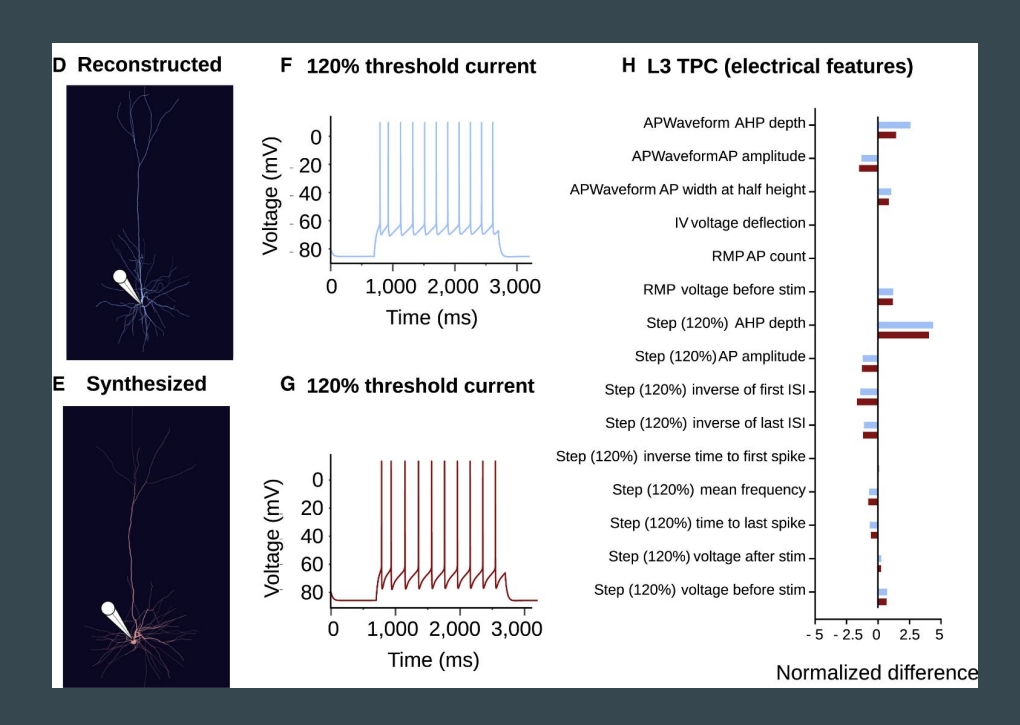
B. Dendritic elongation: during continuation the branch grows based on a segment length and direction. The direction is chosen as a combination of three parameters: randomness, memory (based on the previous directions within a branch), and targeting (based on the initial direction of a branch).



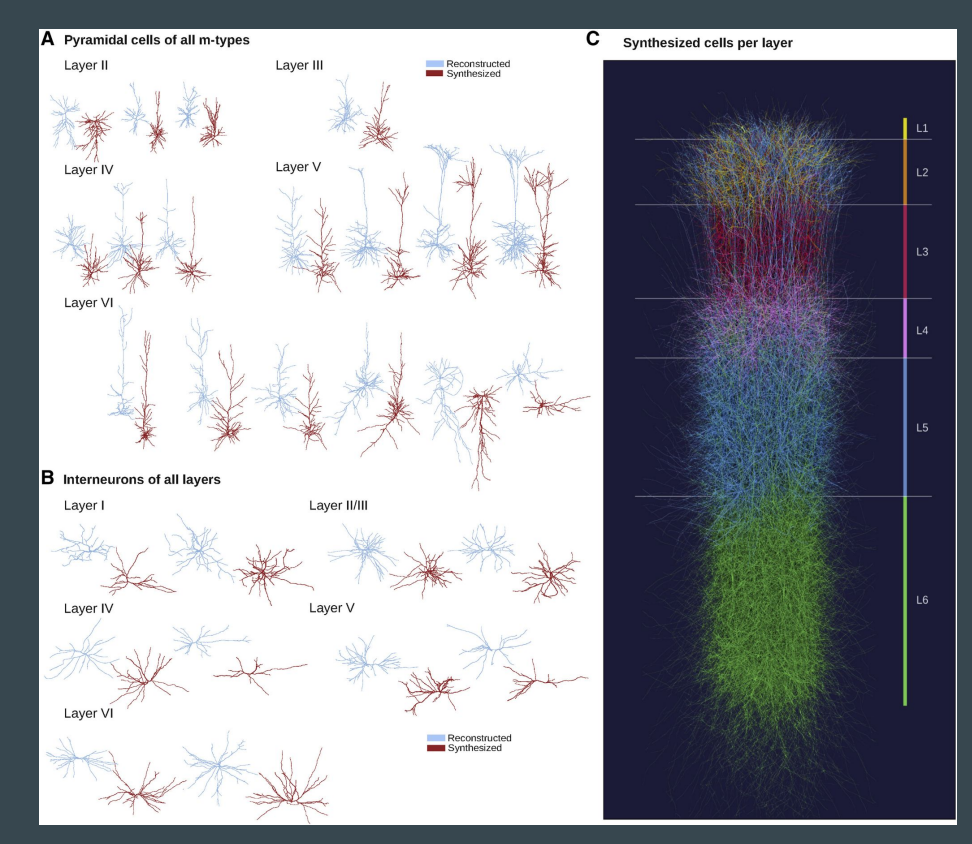
Validation of single-cell morpho-electrical properties. (A) Reconstructed layer 3 tufted pyramidal cells (blue) is used as input for 100 synthesized L3_TPCs (red). (B) Comparison of topological persistence diagrams of the reconstructed cell and 100 synthesized cells. (C) Comparison of 19 dendritic morphometrics (normalized based on the mean morphological feature values for the L3_TPC population) for a reconstructed and a synthesized cell.



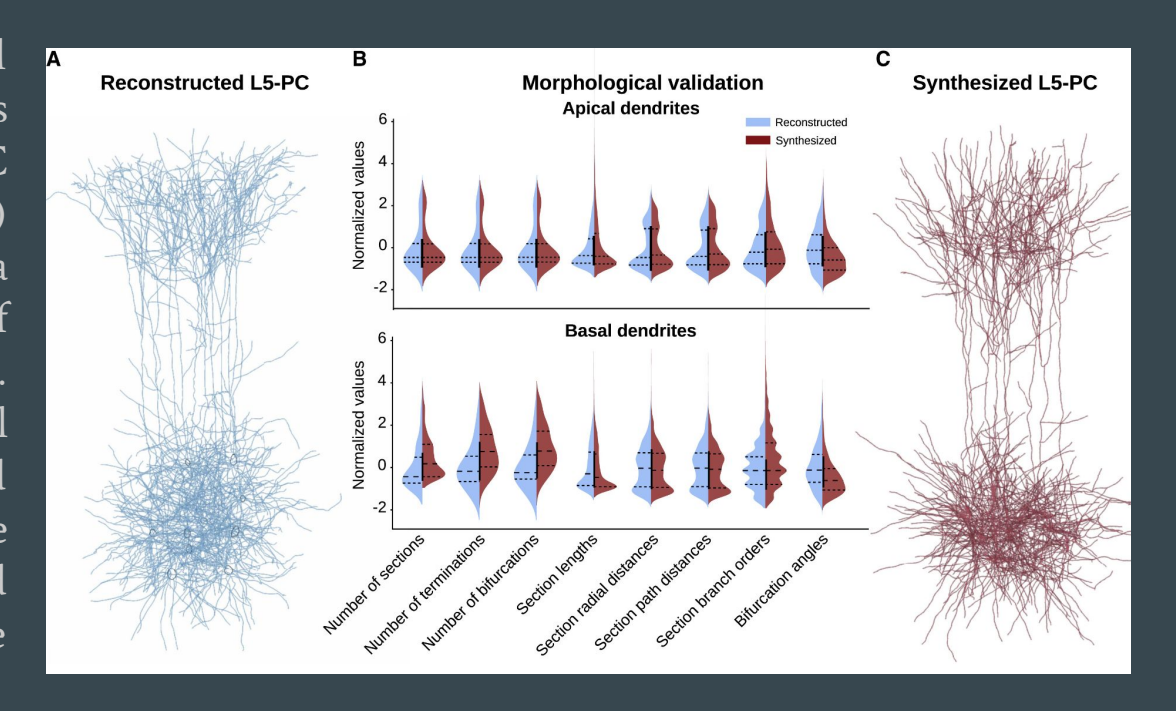
(D and E) The reconstructed (D) and synthesized cell (E) electrically simulated according to a model optimized on the electrical properties of L3_TPC cells. (F and G) The electrical response (120%) threshold current step) of the reconstructed cell (F) is compared with the synthesized cell's (G). (H) Comparison of 15 electrical properties of dendrites (normalized based on the mean electrical feature values for the L3_TPC population.



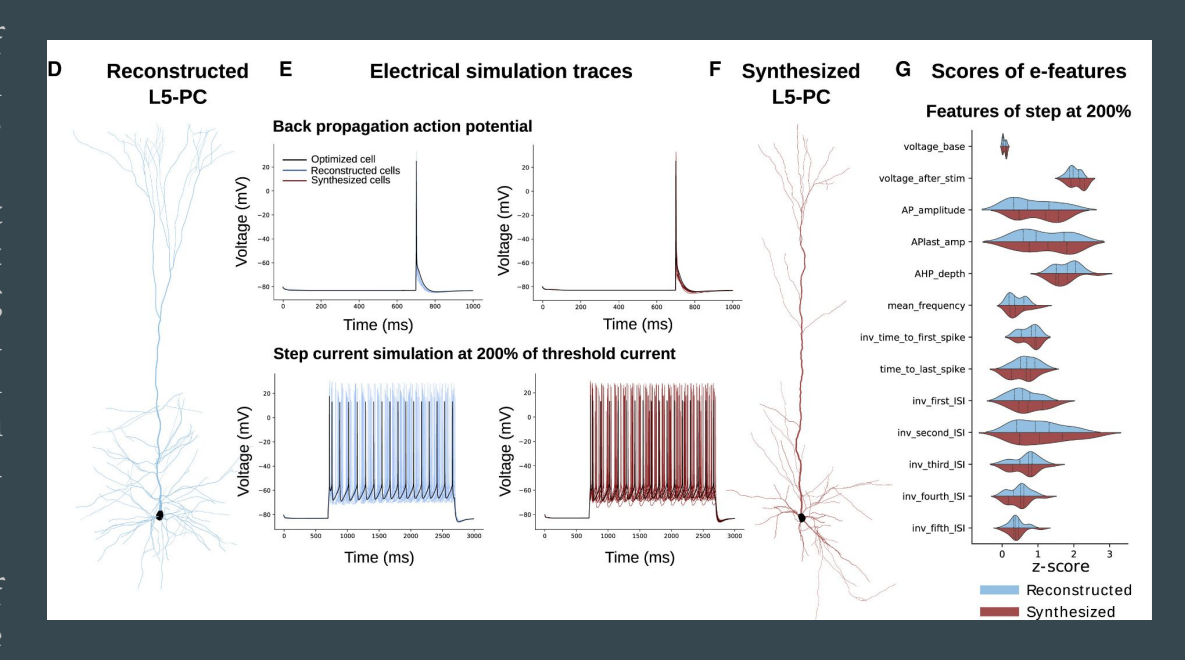
Comparison of reconstructed and synthesized dendritic shapes (A) Reconstructed (blue) and synthesized (red) pyramidal cell dendrites of all rodent cortical m-types from layers 2 to 6. (B) Reconstructed (blue) and synthesized (red) dendrites of rodent cortical interneurons of layers 1 to 6. Not all interneuron morphology types are reported, as they differ mainly in their axonal branches and not significantly on the basal dendrites, as illustrated. (C) A cortical column of synthesized dendrites of all layers, colors correspond to cortical layers from 1 to 6.



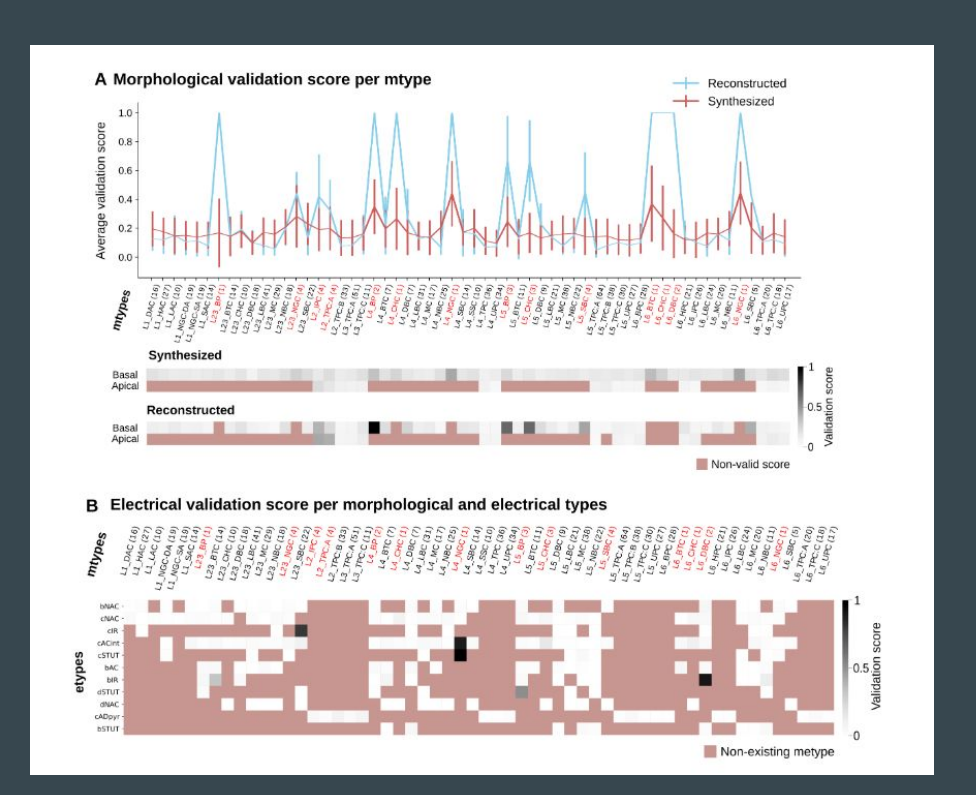
Morphological and electrical validation of synthesized dendrites (A–F) A set of L5_TPC:C reconstructions (A) (blue, 30 cells) is used as input to generate a population of synthesized cells of the same type (C) (red, 100 cells). The violin plots of morphological properties (B) for apical (top) and basal (bottom) dendrites of the reconstructed cell (in blue) and the synthesized cells (in red) are reported.



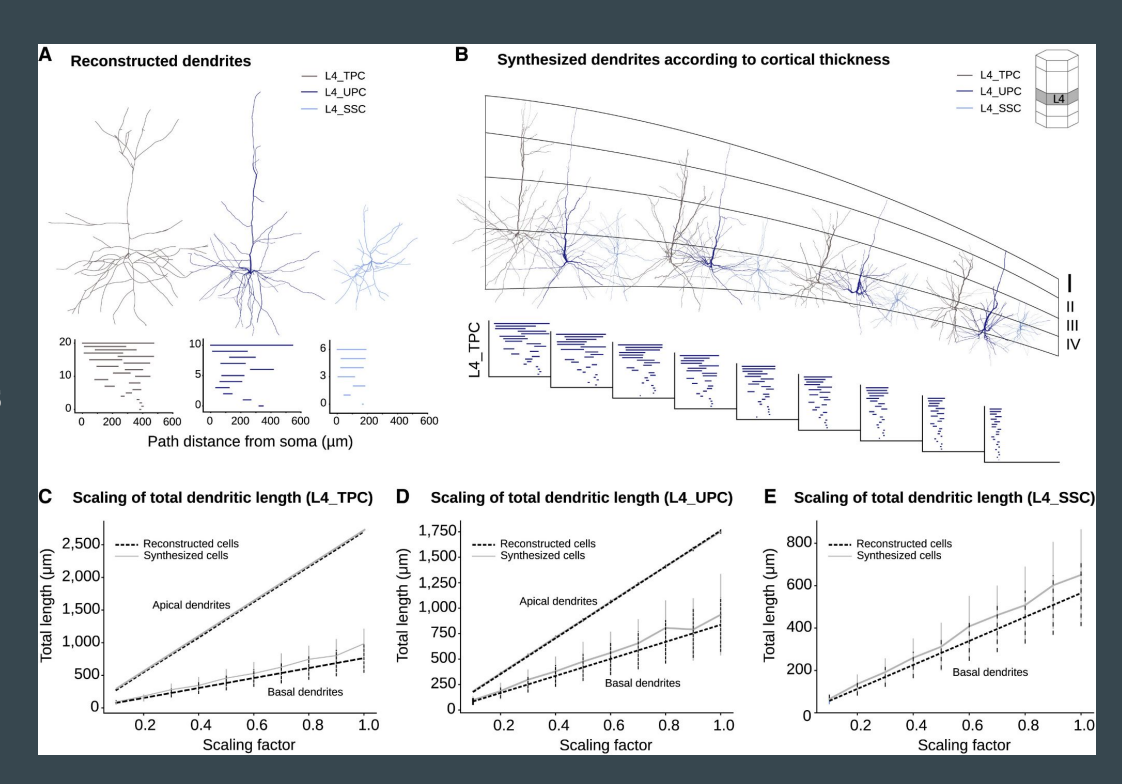
Electrical traces (E) from simulation of ten reconstructed (D) (blue) and synthesized morphologies (F) (red) are compared with the reference trace for the optimized model (black). Step current simulation at 200% of threshold current illustrates similar frequency in firing patterns of synthesized and reconstructed cells. Back-propagation action potential illustrates similar spike shape between reconstructed synthesized and morphologies. (G) Validation of the electrical features extracted from the traces of step current simulation (E) of reconstructed (blue) synthesized (red) cells using Z scores with respect to experimental features.



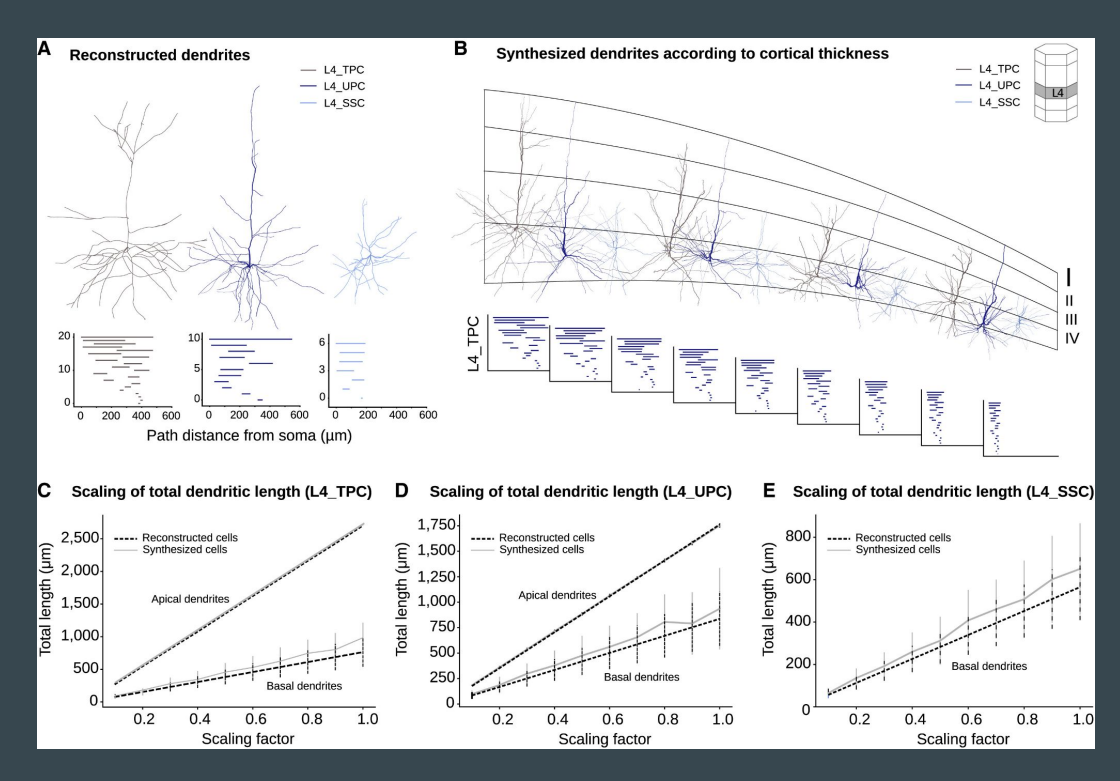
Morpho-electrical validation. A. Morphological validation of synthesized cells per mtype (the sample size is shown in parenthesis, mtypes with fewer than 5 exemplars are annotated in red). Validation (MVS) scores averaged over all features for each mtype (top) for reconstructed (blue) and synthesized (red) cells. Comparison of average (MVS) scores between reconstructed - synthesized cells (top) and within reconstructed cells (bottom) for basal and apical dendrites. B. MVS scores between z-scores of reconstructed and synthesized cells' electrical features for each morpho-electrical type.



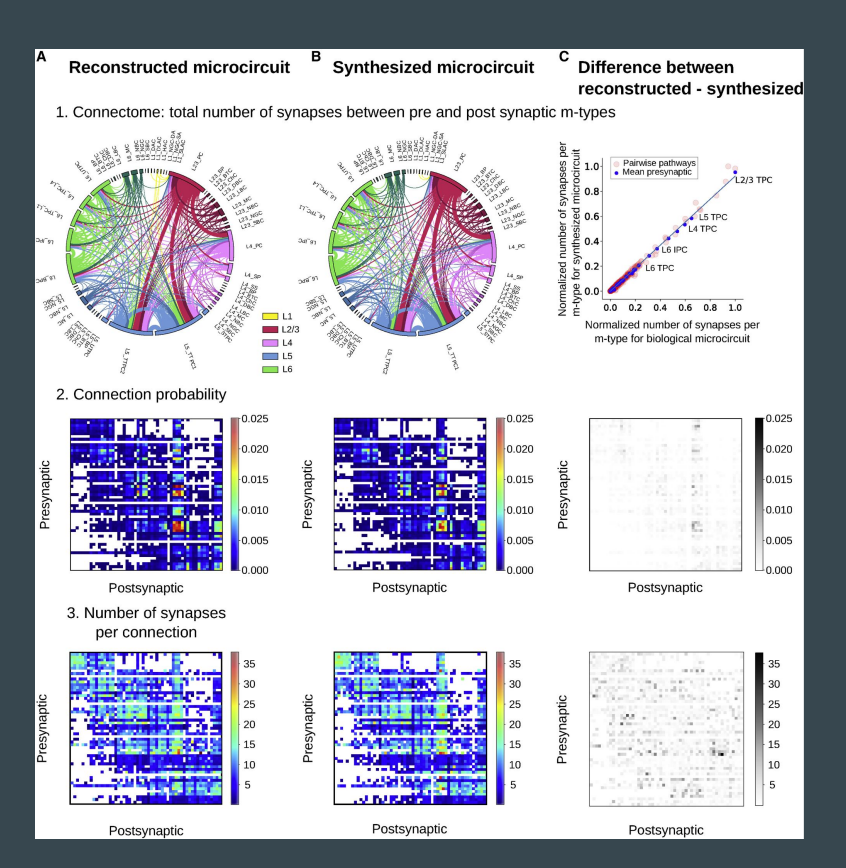
Generalization of topological synthesis for varying cortical thickness. (A) Exemplar biological reconstructions of three layer 4 pyramidal cell types: L4_TPC (gray), L4_UPC (deep blue), L4_SSC (light blue), and the corresponding persistence barcodes, used as synthesis input. (B) Scaling of input persistence barcodes and resulting synthesized dendrites ([1.0, 0.8, 0.6, 0.5] of original barcodes). The scaled (from 1.0 to 0.2) barcodes of synthesized L4_TPC apicals presented at the bottom.



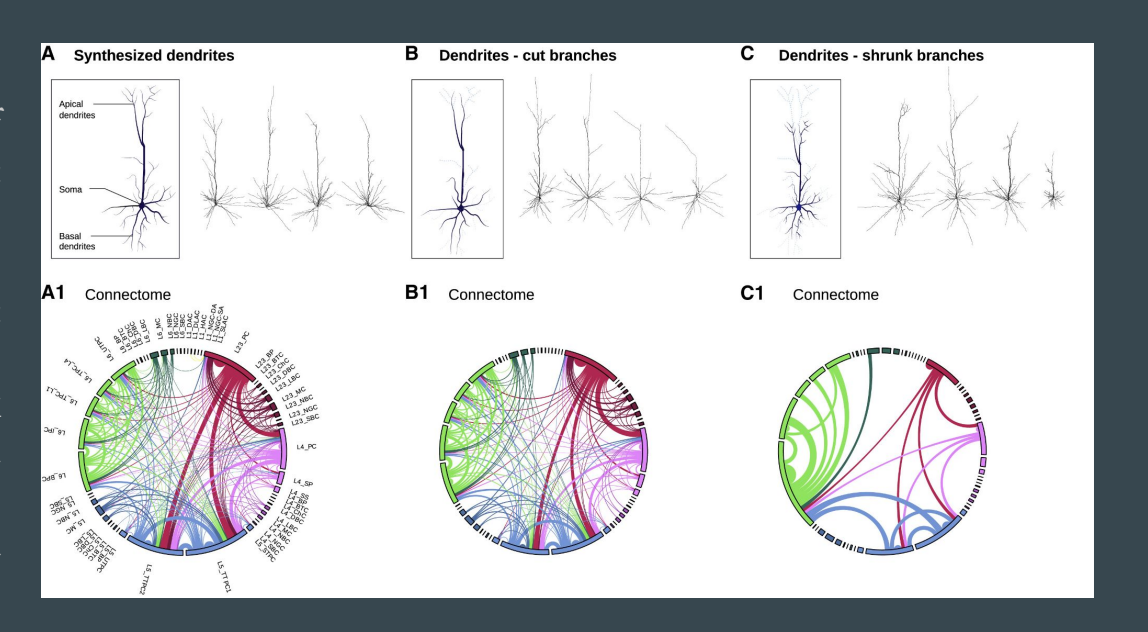
(C–E) Total dendritic length of layer 4 cells, as a function of shrinkage factor for basal (bottom) and apical (top) dendrites compared expected values of scaled biological lengths (black dashed, computed as scaling factor multiplied by total length of reconstructed dendrites) and synthesized (gray continuous) dendrites of L4_TPC (C), L4_UPC (D), and L4_SSC (E). Note that L4_SSC do not have apical dendrites even though they are excitatory cells, therefore only basal dendrite statistics are shown.



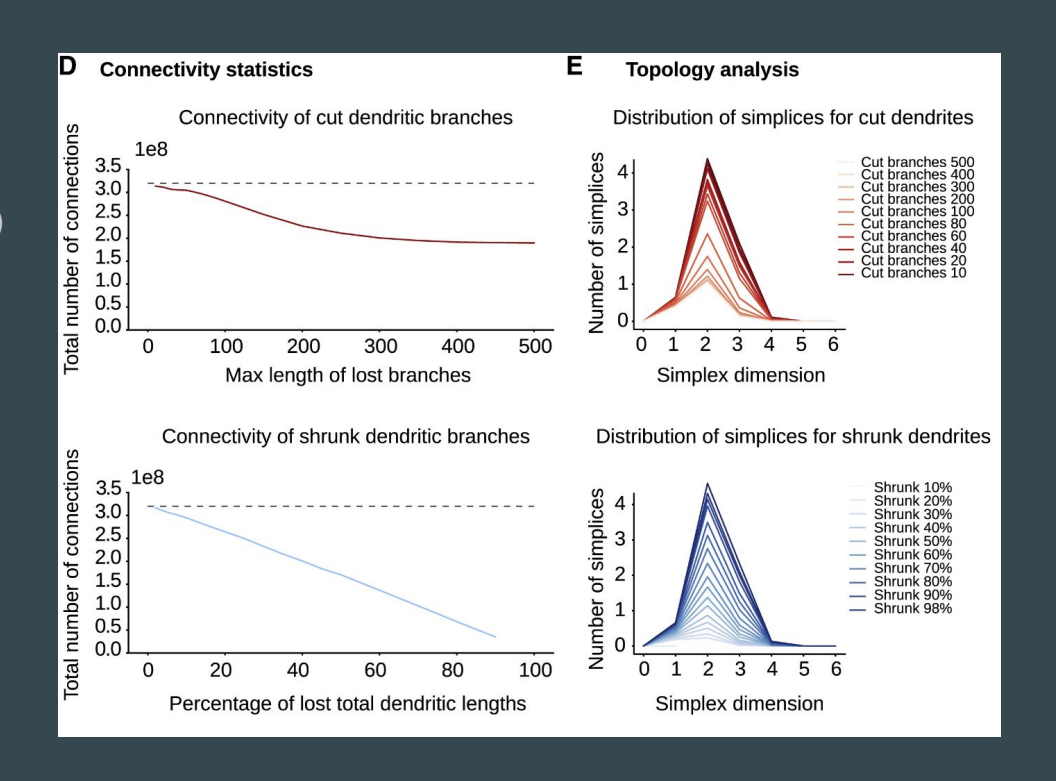
Connectivity of synthesized and reconstructed networks. (A) The connectivity properties of a reconstructed microcircuit (Markram et al., 2015). (B) The connectivity properties of a microcircuit of fully synthesized dendrites, and reconstructed axons. (C) Difference between reconstructed and synthesized microcircuits. (1) The connectomes of the microcircuits grouped by m-type. (2) Connection probability. (3) Synapses per connection.



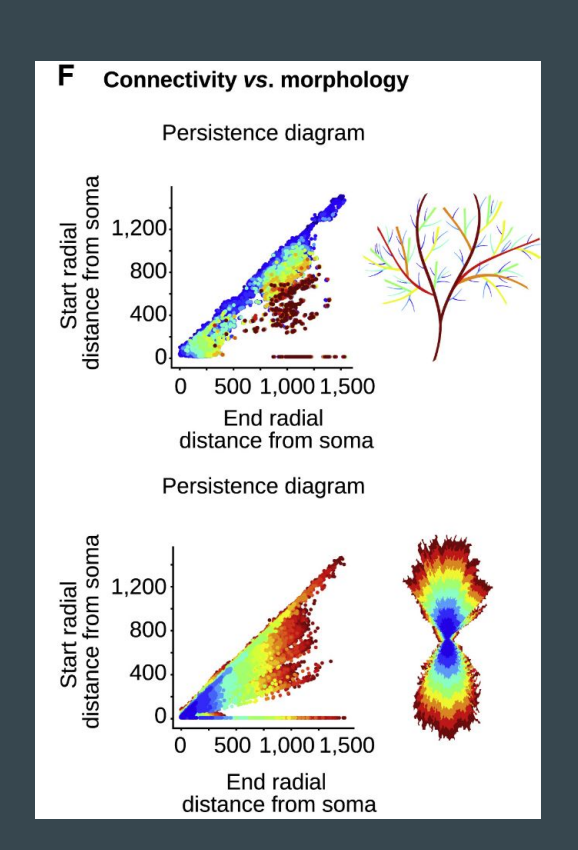
Medical applications. (A–C) Connectivity of synthesized networks based on structural alterations of dendritic morphologies. Schematic representation and examples of layer 5 synthesized pyramidal cells (A), in comparison with cut dendritic branches (B) (lengths above 10, 100, 200, and 400 µm), and shrunk dendrites (C) (98%, 90%, 60%, and 30%). Connectome (presented in subpanel 1) of each synthesized microcircuit: (A) synthesized, (B) cut branches of lengths above 400 µm, (C) shrunk dendrites 10%.



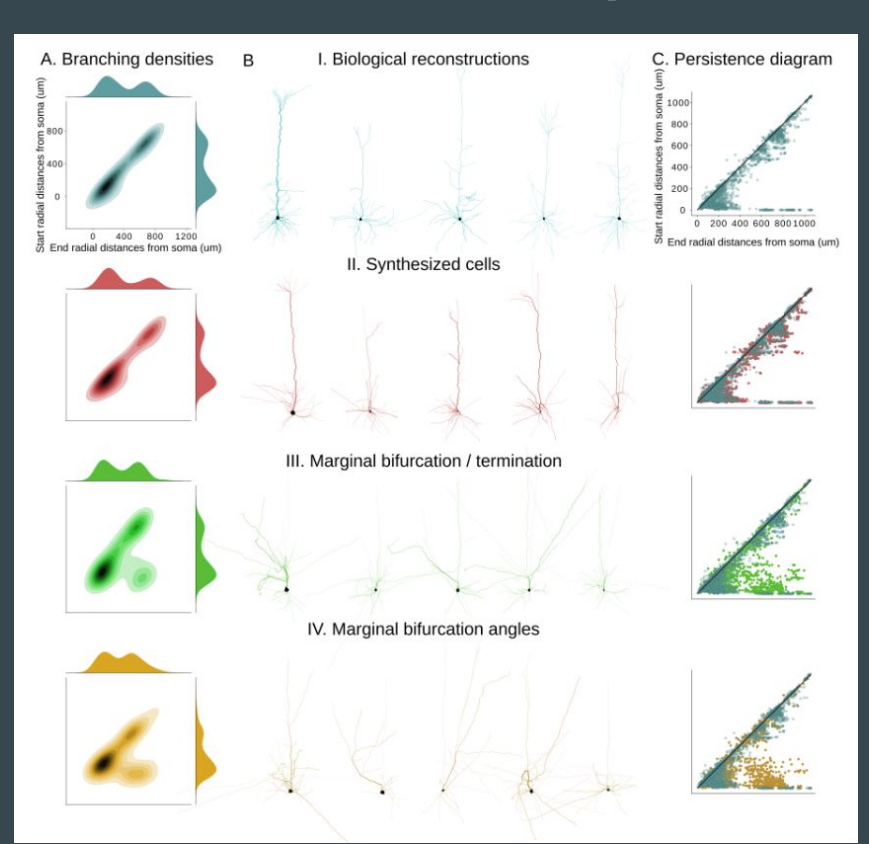
(D) Total number of connections for alterations of type B (red) and C (blue) compared with synthesized network A (black). (E) Topological analysis of corresponding networks; distribution of directed simplices for alterations of type B (red, top) and C (blue, bottom).



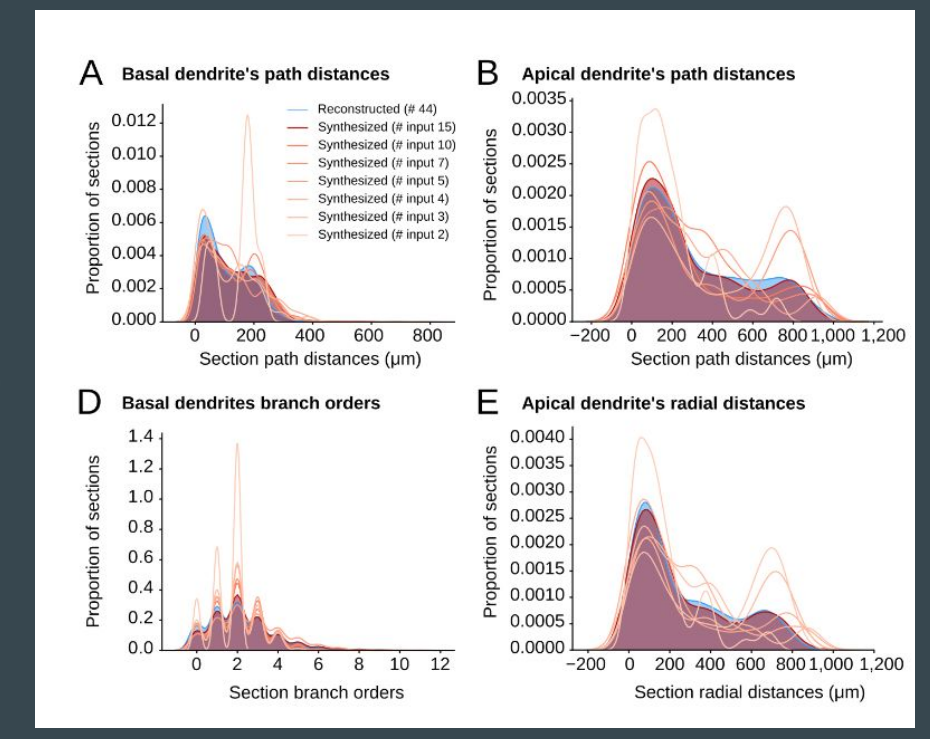
(F) Morphological characteristics and connectivity with respect to alterations of type B (top) and C (bottom). The main branches form the majority of connections (top) and larger dendritic extents (bottom) form more connections. Colormap corresponds to normalized number of connections: from maximum number of connections (3.5 \times 108 in red) to minimum (107 in blue).



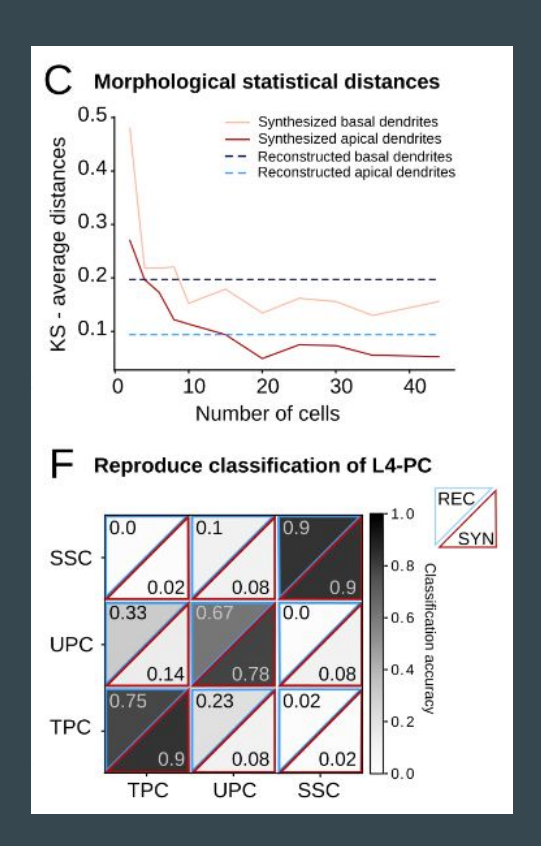
Comparison of synthesis methods. Comparison of synthesized cells for different synthesis methods. A. Density and marginal projections of persistence diagrams for reconstructed cells (I), synthesized cells (II), synthesized without correlation of branching / termination (III), and synthesized without correlation between branching and bifurcation angles (IV). B. Examples for the same data. C. Respective persistence diagrams.



Morphological diversity. Comparison of dendrites from 44 reconstructed L4 TPC cells (in blue) to synthesized dendrites (based on subsets of increasing numbers of cells from the original population used as inputs: from 2 to 15, red shades from lighter to darker). Comparison of path distance (A, direct input) and branch order (B, emergent property) for basal dendrites. Comparison of path distances (D, direct input) and radial distance (E, emergent property) for apical dendrites. The original distributions are well approximated by a subset of input cells (15 out of 44).



C. Average statistical (Kolmogorov-Smirnov) distance for numerous morphometrics, within reconstructed cells (in blue) and between reconstructed and synthesized cells (in red) as a function of increasing synthesis inputs. F. TMD based classification of three L4 PC types for reconstructed (top left, blue) and synthesized (bottom right, red) cells. Classification accuracy is same or higher for the synthesized population.



Questions?